Barker, P.F., Camerlenghi, A., Acton, G.D., and Ramsay, A.T.S. (Eds.)
Proceedings of the Ocean Drilling Program, Scientific Results Volume 178

5. Palmer Deep Composite Depth Scales for Leg 178 Sites 1098 and 1099[1]

Gary D. Acton,[2] Charles J. Borton,[3] and the Leg 178 Shipboard Scientific Party[4]

ABSTRACT

Multiple holes were cored at Ocean Drilling Program Leg 178 Sites 1098 and 1099 in two subbasins of the Palmer Deep in order to recover complete and continuous records of sedimentation. By correlating measured properties of cores from different holes at a site, we have established a common depth scale, referred to as the meters composite depth scale (mcd), for all cores from Site 1098. For Site 1098, distinct similarities in the magnetic susceptibility records obtained from three holes provide tight constraints on between-hole correlation. Additional constraints come from lithologic features. Specific intervals from other data sets, particularly gamma-ray attenuation bulk density, magnetic intensity, and color reflectance, contain distinctive anomalies that correlate well when placed into the preferred composite depth scale, confirming that the scale is accurate. Coring in two holes at Site 1099 provides only a few meters of overlap. None of the data sets within this limited overlap region provide convincing correlations. Thus, the preferred composite depth scale for Site 1099 is the existing depth scale in meters below seafloor (mbsf).

INTRODUCTION

During Ocean Drilling Program (ODP) Leg 178, two sites were drilled in the Palmer Deep, a basin on the continental shelf of the Antarctic Peninsula (Barker, Camerlenghi, Acton, et al., 1999). The Palmer Deep

[1] Acton, G.D., Borton, C.J., and the Leg 178 Shipboard Scientific Party, 2001. Palmer Deep composite depth scales for Leg 178 Sites 1098 and 1099. *In* Barker, P.F., Camerlenghi, A., Acton, G.D., and Ramsay, A.T.S. (Eds.), *Proc. ODP, Sci. Results,* 178, 1–35 [Online]. Available from World Wide Web: <http://www-odp.tamu.edu/publications/178_SR/VOLUME/CHAPTERS/SR178_05.PDF>. [Cited YYYY-MM-DD]
[2] Ocean Drilling Program, Texas A&M University, 1000 Discovery Drive, College Station TX 77845, USA. acton@odpemail.tamu.edu
[3] Chemistry Department, Hamilton College, 198 College Hill Road, Clinton NY 13323, USA.
[4] Shipboard Scientific Party addresses can be found under "Shipboard Scientific Party" in the preliminary pages of the volume.

Initial receipt: 3 November 1999
Acceptance: 2 March 2001
Web publication: 6 June 2001
Ms 178SR-202

contains three subbasins, the deepest of which is over 1400 m deep, roughly 1000 m deeper than the surrounding shelf (Fig. F1). Thick Holocene sedimentary sections were recovered from both drill sites. Site 1098 lies within Basin I, the smallest and shallowest of the three subbasins, at a water depth of 1011 m. Site 1099 lies within Basin III, the largest and deepest of the subbasins, at a water depth of 1400 m.

Multiple holes were cored at both sites with the advanced piston corer (APC), with the goal of recovering as complete a section as possible given time limitations. At Site 1098, three holes were cored through the roughly 46-m-thick sedimentary fill overlying acoustic basement. Hole 1098A was drilled to 45.9 meters below seafloor (mbsf) with 45.78 m of sediment recovered (99.74% recovery); Hole 1098B was drilled to 43.0 mbsf with 44.66 m of sediment recovered (103.86% recovery); and Hole 1098C was drilled to 46.7 mbsf with 46.3 m of sediment recovered (99.14% recovery).

At Site 1099, two holes were cored through the upper 107.5 m of the ~260-m-thick sediment fill overlying basement. Owing to time constraints, the interval was effectively cored only once with the two holes overlapping only 2.3 m in the meters below seafloor depth scale. The upper 62.3 m of section was cored in Hole 1099A, and the interval from 60.0 to 107.5 mbsf was cored in Hole 1099B.

The primary goal of this study is to construct a common depth scale for the three holes at Site 1098. Secondarily, we illustrate that a common depth scale cannot be accurately constructed for the two holes at Site 1099.

The depth to the top of each core is originally estimated from a drill-pipe measurement. These drill-pipe measurements, along with curation procedures, establish a unique depth scale in meters below seafloor for the cores from each hole (e.g., see the "Explanatory Notes" chapter in Barker, Camerlenghi, Acton, et al., 1999).

The mbsf depths differ from true depths for several reasons. Ship motion, heave, and deviation of the drill hole from vertical can all cause errors in drill-pipe measurements. Depth errors may also result from biases in core recovery estimates, which commonly exceed 100% for APC cores. These artificially high recovery percentages probably result from decompression of sediments (Farrell and Janecek, 1991; Hagelberg et al., 1995; MacKillop et al., 1995; Moran, 1997), entrance of excess sediment into the core barrel as some of the sediment displaced by the walls of the coring shoe is forced inward (p. 93–96 of Hvorslev, 1949), and curation practices, in which soupy core material commonly occurring at the top of many cores is curated as part of the core. In reality, much of the soupy material results from sediment falling into the hole or from sediment being stirred at the bottom of the hole. This happens as the roller-cone bit, which is part of the bottom-hole assembly (BHA), advances from the top of the previously recovered core to the top of the core that is next to be recovered. If the ship heaves upward as the piston strokes into the sediment, then the debris in the hole can be recovered. Additional expansion of the upper part of each core can occur because the top of the core is exposed to circulating water, particularly as the water jets from the BHA are cleaning out the hole. Incomplete recovery also results in potential depth errors because ODP curation convention assumes the top of the core corresponds to the top of the cored interval. Similarly, duplicate recovery within a hole, where the piston corer repenetrates the same sediment sequence either by piercing the side wall of the borehole or by a lateral shift of the BHA in very water saturated and unconsolidated sediment, can result in depth biases of several

F1. Bathymetric map of Palmer Deep showing Leg 178 drill sites, p. 15.

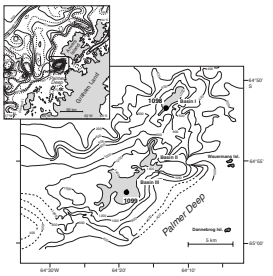

meters, as was shown by Robinson (1990). Depth errors also result from core deformation, such as "suck-in" that occurs when sediment is sucked up into the core liner. Smaller depth errors result from minor core distortion that occurs to some degree in most APC cores, such as bowed or sheared sediment near the core liner caused by friction as the sediment passes through the coring shoe and into the core liner (p. 93–100 of Hvorslev, 1949).

Given these factors, one would expect misalignment of correlative features between holes at a site. Thus, a continuous horizontal feature collected in several holes at a site, which in the absence of local bathymetric variations would have the same true depth in each hole, will likely have different mbsf depths. The offset of such features in the mbsf depth scale may be only several centimeters or could be a few meters, though rarely more than 10 m, based on observations from past Deep Sea Drilling Project (DSDP) and ODP legs (e.g., Leg 94 [Ruddiman et al., 1987; Ruddiman, Kidd, Thomas, et al., 1987], Leg 108 [Ruddiman, Sarnthein, Baldauf, et al., 1988], Leg 111 [Alexandrovich and Hays, 1989], Leg 115 [Robinsion, 1990], Leg 117 [Murray and Prell, 1991; deMenocal et al., 1991], Leg 121 [Farrell and Janecek, 1991], Leg 138 [Hagelberg et al., 1992, 1995], Leg 154 [Curry, Shackleton, Richter, et al., 1995], Leg 162 [Jansen, Raymo, Blum, et al., 1996], Leg 167 [Lyle, Koizumi, Richter, et al., 1997], Leg 172 [Keigwin, Rio, Acton, et al., 1998], Leg 175 [Wefer, Berger, Richter, et al., 1998], and Leg 177 [Gersonde, Hodell, Blum, et al., 1999]).

A common or composite depth scale overcomes many of the inadequacies of the mbsf depth scale, allowing core data from one hole to be compared or combined ("spliced") directly with core data from other holes at the same site (e.g., Ruddiman et al., 1987; Ruddiman, Sarnthein, Bauldauf, et al., 1988; Alexandrovich and Hays, 1989; Robinson, 1990; Farrell and Janecek, 1991; Hagelberg et al., 1992, 1995; Curry, Shackleton, Richter, et al., 1995; Jansen, Raymo, Blum, et al., 1996; Lyle, Koizumi, Richter, et al., 1997; Keigwin, Rio, Acton, et al., 1998; Wefer, Berger, Richter, et al., 1998; Gersonde, Hodell, Blum, et al., 1999). The construction of composite depth scales is a natural outcome of efforts to obtain complete recovery of sedimentary sections by piston coring two or more offset holes at a site, which began with the use of the hydraulic piston corer during DSDP Leg 68 (Prell, Gardner, et al., 1982) and has become standard practice since APC coring began during DSDP Leg 94 (p. 8–9 of Ruddiman, Kidd, Thomas, et al., 1987; see also Hagelberg et al., 1995, for a history of composite section development). Cores from a single hole will nearly always have some intervals with poor or no recovery or with recovery of sediments that are disturbed during drilling. Even when core recovery is quoted as 100% or higher, gaps of several meters can occur between cores (e.g., Shackleton et al., 1984; Ruddiman et al., 1987; Robinson, 1990; Farrell and Janecek, 1991). By splicing or stacking core intervals from different holes at a site that has been multiply cored, a complete or nearly complete stratigraphic section can be constructed.

DATA

In creating the meters composite depth (mcd) scale, we attempted to ignore data from intervals that were disturbed or distorted by the drilling process (Table T1). This typically includes the uppermost 5–70 cm of nearly every core, which is commonly more water saturated or soupy

T1. Intervals disturbed or distorted by coring, p. 28.

relative to the sediment below. Only in the first core at each hole, particularly at the mudline (sediment/water interface), would we expect to see such poorly consolidated sediments. We also avoided other distortions, such as gas voids and deformed sediments. Hole 1098C contained additional data gaps caused by the removal of a 5-cm-long interstitial water (IW) sample from the end of each section prior to the measurement on the multisensor track (MST).

The primary data sets used are those collected during Leg 178 with (1) the MST, from which we use the magnetic susceptibility and density that were measured every 2 cm; (2) the Minolta color scanner, from which we use the color reflectance parameters L*, a*, and b* that were measured every 2 cm; and (3) the long-core cryogenic magnetometer, from which we use the inclination and intensity measured every 5 cm (Barker, Camerlenghi, Acton, et al., 1999). Susceptibility or paleomagnetic data collected within 5 cm of the end of each section are ignored, because the sensors that measure these parameters average over several centimeters of core, and so measurements near the ends of the sections are biased. Additional constraints come from core photos and core descriptions.

METHOD

Composite Depth Scale

We have constructed a composite depth scale using the program SPLICER, developed by Peter deMenocal and Ann Esmay (SPLICER version 2.2 is available on the World Wide Web from the Borehole Research Group at Lamont Doherty Earth Observatory, Columbia University, at **http://www.ldeo.columbia.edu/BRG/ODP**). This program allows data from several holes at a site to be viewed and manipulated simultaneously. Correlations are made within the program by selecting data from one core from one of the holes and then overlying it with data from another core from a different hole. The data being compared can be shifted vertically relative to each other until a preferred correlation is made. These depth offsets are recorded in a SPLICER "affine" table. After correlating all cores between holes, the end result is an affine table that gives the depth shift that needs to be applied to the mbsf depth scale for each core to place the cores into the composite depth scale. The depth of each core can then be computed in meters composite depth, as presented in Table **T2** for Site 1098.

T2. Composite depth scale, Site 1098, p. 29.

Correlation typically begins with cores from the top of the sedimentary section and proceeds downhole. For sites with multiple holes, each cored from the seafloor to some depth, the initial core selected for the top of the composite section (0 mcd) would ideally be one in which the mudline and several meters of core were recovered with minimal coring deformation. Features from cores from the other holes would then be aligned with features from the initial core by applying depth shifts, and so on downhole. Because core expansion is common, the correlation process results in mcd scales that are commonly expanded by about 2%–20% from the true depth (e.g., Farrell and Janecek, 1991; Hagelberg et al., 1995; MacKillop et al., 1995). Hence, the composite depth scale should not be confused with a true depth scale or even a best estimate of a true depth scale (see discussion in Harris et al., 1995). Instead, it is a common depth scale that provides a stratigraphic framework for other studies.

To determine the quality of the correlation, we used visual comparison as well as the calculated correlation coefficient shown graphically within SPLICER. The correlation coefficient is determined by cross-correlating the data from two cores. Its value ranges from +1 to –1, and the window over which it is calculated is adjustable. In nearly every case, we used the default window length of ±2 m above and below a selected tie point. Occasionally, we reduced this to ±1 m to focus on specific features or to avoid features related to coring disturbance.

No expansion or compression of one core or core interval relative to others is permitted within SPLICER. Because of this restriction, it is not always possible to exactly align every anomaly with similar anomalies in other cores. Second-order correlation of that nature can be best accomplished by using programs like ANALYSERIES (Paillard et al., 1996) or by using methods like inverse correlation (Martinson et al., 1982) to adjust the first-order correlation accomplished with SPLICER.

Spliced Cores

A splice is constructed by combining discrete intervals from the cores from different holes to give one continuous sedimentary section for the site. The splice uses portions of data from different holes after the data have been converted to the mcd scale. Typically, a cored interval selected to be part of the splice will have the least drilling disturbance and the fewest gas voids, IW samples, and irregularities when compared with the same depth interval from other holes. We have produced a "splicertable," which gives the intervals that are preferred for the spliced sedimentary section (Table **T3**).

COMPOSITE DEPTH SCALE FOR SITE 1098

We examined several data sets initially to see which data could be most easily correlated from one hole to the next. We envisioned creating independent composite depth scales using different data sets in the hope that the scales would be very similar and that a best-fit composite depth scale could then be derived. Unfortunately, correlation of several of the data sets from one hole to the next was difficult and in some cases no convincing preliminary mcd scale could be produced. This was especially true for the color reflectance data (lightness [L*], the chromaticity parameters a* and b*, and the 500-nm wavelength signal) and the paleomagnetic inclination, though each of these data sets have a few depth intervals where anomalies can be correlated. The magnetic susceptibility records, on the other hand, contain anomalies that can clearly be correlated from hole to hole over nearly the entire cored interval (Figs. **F2, F3, F4, F5**). The gamma-ray attenuation (GRA) density (Figs. **F6, F7, F8, F9**), magnetic intensity (Figs. **F10, F11**), and the color reflectance parameter a* (Fig. **F12**) data provide several intervals that correlate very well, though not nearly as well overall as the susceptibility data. Hence, our preferred composite scale (Table **T2**) was generated using the susceptibility data. We then applied the mcd scale to the other data sets to confirm that their correlatable anomalies were indeed properly correlated.

Below, we outline the features (lithologic units and anomalies from susceptibility, GRA density, color reflectance, and paleomagnetic inclination and intensity) that we think should be aligned within any com-

T3. Splice tie points, Site 1098, p. 30.

F2. Susceptibility data for Site 1098, p. 16.

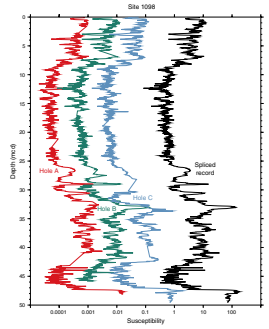

F3. Susceptibility record, 0–8 mcd, p. 17.

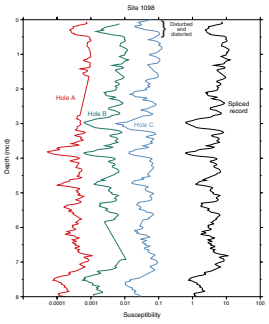

F4. Susceptibility record, 8–20 mcd, p. 18.

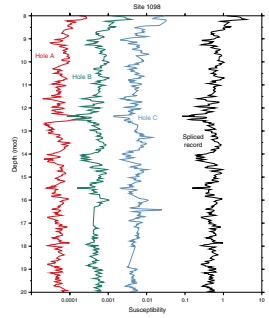

posite depth scale. Our preferred composite depth scale achieves this goal.

Lithologic Features

Two distinctive lithologic subunits (IA and IB) were identified by the Leg 178 sedimentologists (see the "Palmer Deep" chapter in Barker, Camerlenghi, Acton, et al., 1999). The contact between these subunits, as well as two other prominent lithologic contacts, were correlated and used as tie points in the composite depth scale. These contacts are described below, and their positions in each hole are presented in Table T4.

Subunit IA/IB Contact

Subunit IB, which contains more clastic material (ice-rafted debris and pebbles) than the overlying Subunit IA, was defined as occurring from Section 178-1098A-6H-3, 60 cm, to the base of Hole 1098A and from Section 178-1098C-5H-4, 50 cm, to the base of Hole 1098C (Barker, Camerlenghi, Acton, et al., 1999). The boundary between Subunits IA and IB is a zone less than ~20 cm wide, where laminated diatomaceous mud at the base of Subunit IA grades into silty clay with ice-rafted debris and pebbles of Subunit IB. The Subunit IA/IB contact can be correlated between cores with an accuracy of about ±15 cm.

Upper Contact of the Lower Laminated Interval

A laminated diatomaceous mud, ~340 cm thick, occurs at the base of Subunit IA. This lower laminated (LL) interval spans 345 cm in Hole 1098A (interval 178-1098A-6H-1, 15 cm, to 6H-3, 60 cm) and 330 cm in Hole 1098C (interval 178-1098C-5H-2, 25 cm, to 5H-4, 50 cm). In Hole 1098B, only 296 cm of the LL interval was recovered (interval 178-1098B-5H-5, 102 cm, to the bottom of the hole) during coring, which did not penetrate the lower portion of this interval. The upper boundary of the LL interval can be correlated between cores with an accuracy of about ±15 cm.

Homogeneous to Laminated Contact

The distinctive homogeneous to laminated (HL) contact between a laminated diatom ooze and underlying very homogeneous massive diatom ooze (a turbidite unit) occurs within the upper portion of Subunit IA in all three holes (Sections 178-1098A-4H-2, 80 cm [23.20 mbsf]; 178-1098B-3H-6, 40 cm [23.40 mbsf]; and 178-1098C-3H-5, 8 cm [24.28 mbsf]). The contact is sharp and can be easily identified in the core photographs. This contact (at 24.92 mcd), which can be correlated between cores with an accuracy of ±2 cm, provides a key constraint for the composite depth scale.

Magnetic Susceptibility

The magnetic susceptibility record was by far the easiest to correlate. Correlations established using the susceptibility record thus served as the basis for construction of the composite depth scale (Table T2) and the splice (Table T3). Characteristics of susceptibility data important in the correlation are described below.

F5. Susceptibility record, 20–28 mcd, p. 19.

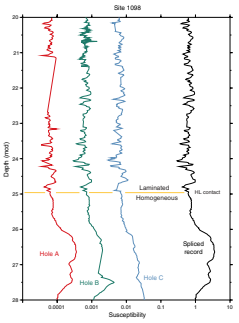

F6. GRA density data for Site 1098, p. 20.

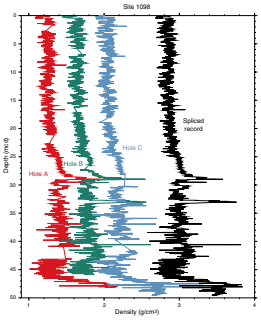

F7. Density record, 0–8 mcd, p. 21.

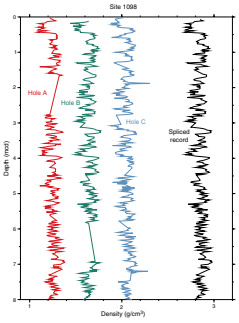

F8. Density record, 20–28 mcd, p. 22.

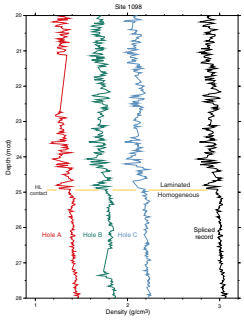

1. The interval with the largest uphole decrease in susceptibility from Hole 1098C (interval 178-1098C-5H-4, 124–138 cm) correlates with the similar interval within Hole 1098A (interval 178-1098A-6H-3, 130–142 cm) (Fig. F2). In this interval, the susceptibility decreases from 2040 to 50 in Hole 1098A, whereas it decreases from 2860 to 920 in Hole 1098C (all susceptibility values are given in raw meter values, which can be converted to SI volume susceptibility units by multiplying by ~0.7 × 10^{-5}). A second decrease occurs in Hole 1098C, about 20 cm further upcore. A slightly better correlation coefficient is obtained by correlating the Hole 1098A decrease with this higher decrease in Hole 1098C (correlation coefficient of 0.86 vs. 0.75 for our preferred correlation), but this misaligns the lithologic Subunit IA/IB contact by ~20 cm.
2. Susceptibility anomalies in the lower laminated intervals (43.19–43.50 mcd) are difficult to correlate with one another (Fig. F2). The susceptibility within this interval is ~10–50 times less than in the nonlaminated intervals. The largest anomalies are associated with dropstones (e.g., the two peaks at Section 178-1098A-6H-1, 48 cm, and 6H-1, 92 cm, occur precisely where two dropstones are present; see the core photo in "Site 1098 Core Descriptions" in Barker, Camerlenghi, Acton, et al., 1999).
3. Above 40 mcd, correlations between holes consistently give correlation coefficients >0.6 and often >0.8. Distinctive sets of anomalies occur throughout, which firmly establishes the accuracy of the composite depth scale (Figs. F2, F3, F4, F5). Difficulties within the 0- to 40-mcd interval arise mainly because some compression or expansion would be required to align every correlatable feature from one hole to another. An example where relative stretching within a core would be required occurs within the 34- to 40-mcd interval. Distinctive anomalies in the 34- to 36-mcd interval in Core 178-1098A-5H correlate precisely with those in Core 178-1098C-4H, but further downcore, at 36–40 mcd, other distinctive anomalies are ~4–12 cm deeper in Core 178-1098C-4H than in Core 178-1098A-5H.
4. Particularly good correlations occur at the HL contact (24.92 mcd). As with the GRA density and color reflectance parameter a* data, the susceptibility data show little variation directly below the contact and large variations above (Fig. F5).
5. The interval from ~16 to 22 mbsf is one of the more difficult to correlate (Figs. F4, F5). Above and below this interval, the correlation is clear; therefore the composite depth scale is well constrained, even within this interval.

GRA Density

1. Correlation coefficients are generally <0.4 for any correlation below ~30 mcd, with few exceptions (Fig. F6). One exception occurs at the very base of Holes 1098A and 1098C, where a gradual decrease in density occurs from the base of both holes to ~3 m uphole. This long-wavelength feature can probably only be correlated to within about ±30 cm (Fig. F9).
2. A distinctive sequence of anomalies, including a large positive density anomaly, at 28.5–29.6 mcd correlates well between

F9. Density record, 40–48 mcd, p. 23.

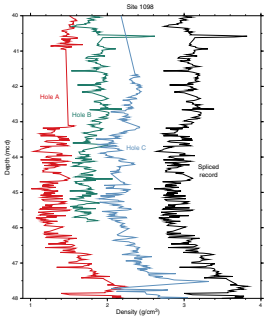

F10. Magnetic intensity data for Site 1098, p. 24.

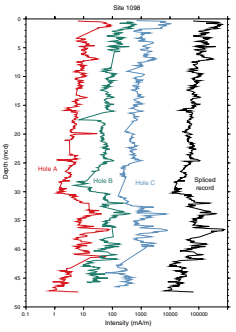

F11. Magnetic intensity data, 33–40 mcd, p. 25.

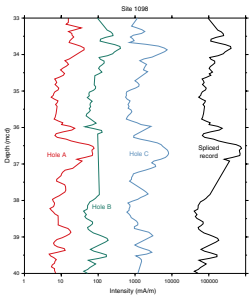

F12. Color reflectance parameter a* data, 20–28 mcd, p. 26.

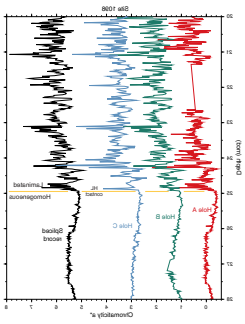

Holes 1098A and 1098B (intervals 178-1098A-4H-4, 138 cm, to 4H-5, 98 cm, and 178-1098B-4H-1, 132 cm, to 4H-2, 92 cm).
3. The density within the very homogeneous massive diatom-ooze interval (24.9–28.0 mcd) in each hole is nearly constant (1.3–1.5 g/cm^3), whereas in the overlying laminated diatom-ooze interval the values show much larger variation (1.3–2.0 g/cm^3). The HL contact is thus associated with a change in the character of the density, which can be correlated well between holes (Fig. **F8**).
4. Correlation coefficients are <0.4 for any correlation from ~16 to 22 mcd.
5. The density records from ~2 to 16 mcd correlate well (correlation coefficients of 0.4–0.6) between all three holes.
6. The anomalies near the mudlines of Holes 1098A and 1098B correlate well, but their correlation with Hole 1098C is poor, probably owing to some coring disturbance (Fig. **F7**).

Color Reflectance Data

1. No unambiguous match can be made with either long- or short-wavelength anomalies from the L*, b*, or 500-nm data, except at the mudline. At the mudline, all three color reflectance parameters correlate very well between Holes 1098A and 1098B only. In general, the best correlation coefficients were <0.4. By smoothing the data, the correlations can be improved a little but overall they are quite poor.
2. Correlation of the color reflectance parameter a* data is mediocre but good enough to illustrate that the composite depth scale aligns distinctive anomalies from one hole to another. In general, the a* data give correlation coefficients of 0.3–0.6. Particularly good correlations are present at the HL contact and a few meters above and below. As with the GRA density data, the a* data show little variation below the contact and large variations above (Fig. **F12**).

Magnetic Intensity

Because the data were only collected every 5 cm and because the cryogenic magnetometer averages over about a 10-cm-long interval, the resolution of the magnetic intensity data is lower than for the susceptibility data. Even so, several features of these data are noteworthy:

1. Correlation coefficients are typically >0.5 for the upper 39 m but correlation is poor below this (Fig. **F10**).
2. An extremely good correlation (correlation coefficients >0.9) of a distinctive set of intensity anomalies occurs in the interval from 33.3 to 39.5 mcd (Fig. **F11**)
3. Above 24 mcd, the correlation of intensity data between Holes 1098B and 1098C is much better than between either of these holes and Hole 1098A (Fig. **F10**).

Magnetic Inclination

Correlation is poor over the entire cored interval, probably owing to coring deformation (shearing occurs on the outer part of the core as the piston corer is shot into the sediments) and measurement artifacts asso-

T4. Lithologic features used for correlating holes, p. 31.

ciated with the weakly magnetized sediments (Brachfeld et al., 2000). As with the intensity data, magnetic inclination correlation between the upper parts of Holes 1098B and 1098C is better than correlations obtained from either of these holes and Hole 1098A. However, none of the features in the inclination data are distinctive enough to help constrain the composite depth scale.

Characteristics of the Preferred Composite Depth Scale

1. The large uphole decreases in susceptibility that occur in a narrow interval near the base of Holes 1098A and 1098C are aligned. Similarly, this scale aligns the largest GRA density anomaly, which occurs within the same interval.
2. The boundary positions between Subunits IA and IB recovered in Holes 1098A and 1098C agree to within 1 cm.
3. The upper boundary of the LL interval in Hole 1098A is 7 cm higher than in Hole 1098B and 15 cm higher than in Hole 1098C. Because the thickness of the LL interval varies between holes, improving the alignment of this boundary would misalign other features that are more distinctive.
4. An extremely good correlation (correlation coefficient >0.9) of magnetic intensity data in the interval from 33.3 to 39.5 mcd is obtained. Offsets >15 cm would degrade this good correlation significantly (correlation coefficients would decrease by ~0.2).
5. The HL contact correlates within ±2 cm in all three holes. Similarly, the distinctive anomalies in GRA density, color reflectance parameter a*, and susceptibility at this contact all provide confirmation that the composite depth scale is accurate and can be precisely constrained in this interval.
6. The composite depth scale requires overlap of 44 cm between Cores 178-1098B-4H and 5H. This overlap can be explained, perhaps entirely, by the 40–45 cm of disturbed sediment at the top of Core 5H.
7. Core 178-1098C-1H overlaps Core 2H by 14 cm. Again, the top 70 cm of Core 2H is disturbed, so this small overlap is not unexpected.
8. Core 178-1098C-1H is shifted up 10 cm from its mbsf depth. This shift can be explained by the 30 cm of coring disturbance that occurs at the top of this core.
9. The color reflectance (L*, a*, b*, and 500-nm signal), susceptibility, and density data sets from the mudlines in Holes 1098A and 1098B agree very well. Owing to coring disturbance of the mudline in Hole 1098C, which is visible in the core photo, the data sets from Hole 1098C correlate poorly with those from Holes 1098A or 1098B.
10. Overall, there are numerous characteristic anomalies in the magnetic susceptibility data that correlate well from one hole to another.

Spliced Data for Site 1098

We have selected intervals for the splice using the susceptibility record and core photos exclusively (Table T3). Our splice avoids using core tops, voids, and data gaps when possible. We also avoided using

data from Section 178-1098B-3H-3, because the susceptibility record for this section contained high-frequency noise not present in core sections above or below.

The splice was constructed from the susceptibility record and is not optimized for other data sets. It should, however, give representative composite records for the other data sets. In rare cases, the other data sets may have missing values within the spliced intervals, owing to the peculiarities of the instruments used during the cruise or the selection criteria used to cull data (e.g., interval 36.9–38.8 mcd for the spliced intensity record in Fig. **F11**). For example, an interval that may have been slightly disturbed by coring may have been considered unacceptable for paleomagnetic remanence measurements but acceptable for magnetic susceptibility, color reflectance, and other measurements. Another artifact that may occur in the composite records for the other data are discontinuities or jumps located at the splice tie points.

Spliced data sets for color reflectance parameter a*, GRA density, magnetic intensity, and susceptibility are included in Tables **T5, T6, T7,** and **T8.** Other data sets converted to the mcd scale can be retrieved from the ODP Janus database on the World Wide Web.

T5. Spliced magnetic susceptibility data, p. 32.

T6. Spliced GRA density data, p. 33.

T7. Spliced magnetic intensity data, p. 34.

T8. Spliced color reflectance parameter a* data, p. 35.

Expansion of the Coring Record

As is typically the case for composite depth scales (see references in **"Introduction,"** p. 1), the total length of the cored interval is expanded by up to ~10% (Fig. **F13**). Sedimentation rates computed from the Site 1098 mcd scale will also be artificially high by up to 10%.

F13. Expansion of depth that occurs for the mcd scale relative to the mbsf scale, p. 27.

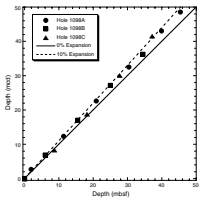

COMPOSITE DEPTH SCALE FOR SITE 1099

Given the minimal overlap at Site 1099, correlating Hole 1099A with Hole 1099B should have been a simple task. Unfortunately, the upper 5 m of core from Hole 1099B has numerous small gas voids and the upper 70 cm is water saturated with a very soupy interval from 52 to 66 cm. The soupy interval produces large anomalies in several of the data sets, particularly in color reflectance parameters a* and b*. Any correlation should, therefore, avoid using at least interval 178-1099B-1H-1, 0–70 cm.

We found that none of the data examined from the upper part of Hole 1099B, which includes magnetic susceptibility, GRA density, and color reflectance (L*, a*, and b*), appears to correlate well with data from the lower few meters of Hole 1099A. One of the better correlations, though not convincing by any means, is obtained from the color reflectance parameter b* data with no depth offset for Hole 1099B relative to Hole 1099A. Given our inability to find any convincing anomalies that suggest that a depth shift was required, we consider the best composite depth scale to be that obtained by using the mbsf scale already available.

In the overlap region, the best splice is then obtained using data from Hole 1099A because there is little or no coring disturbance as opposed to the disturbance visible in the upper 5 m of Hole 1099B.

COMPARISON WITH DEPTH SCALES COMPLETED DURING LEG 178

The composite depth scales presented here differ in important ways and supersede the preliminary versions completed during Leg 178. In particular, time limitations during Leg 178 prevented extensive analysis of many of the data sets, including the lithology and several of the magnetic and physical properties data sets. In contrast, the new depth scales incorporate lithologic constraints and examine a larger array of data sets, allowing us to establish which data sets provide the best correlation and which data should be avoided. For example, the composite depth scale for Site 1098 developed during Leg 178 did not rely on the magnetic susceptibility as a constraint. Here, we have shown that this data set contains many diagnostic anomalies that aid in correlating Holes 1098A, 1098B, and 1098C.

CONCLUSIONS

Distinct similarities in the susceptibility records obtained from the three holes at Site 1098 provide tight constraints for a Site 1098 composite depth scale. Additional constraints come from lithologic features. Specific intervals from other data sets contain distinctive anomalies that correlate very well when placed into the preferred composite depth scale, confirming that the scale is accurate. Shipboard data collected from Site 1098 cores and placed into our mcd scale can be obtained from the ODP Janus database, which is available on the World Wide Web.

Coring in the two holes at Site 1099 provided only a few meters of overlap. None of the data sets within this limited overlap region provide convincing correlations. Thus, the preferred composite depth scale is the existing mbsf scale.

Composite scales, such as established here, represent first-order correlation between holes at a site upon which higher-order depth scales can be built. Smaller-scale features, such as individual lamina or sets of laminae, may not correlate exactly given the restriction that neither compression nor expansion of the length of individual cores was allowed in developing the mcd scales. For Site 1098, sets of laminae, as well as centimeter-scale variations in physical and magnetic properties, will likely be correlatable between holes and should naturally lead to fine-scale adjustments in the composite scale. Several other Leg 178 studies suggest such depth adjustments, most of which align features and data not considered in this study or which require compression or expansion of the mcd depth scale (Brachfeld et al., 2000; Pike et al., **Chap. 18,** this volume; Nederbragt and Thurow, **Chap. 3,** this volume). In some cases, these adjustments resulted in second-order improvements to the mcd depth scale, whereas in other cases they misaligned features that we consider robust. Through our illustrations, tables, and discussion of individual data sets, we hope to establish criteria that will guide future adjustments to depth scales for Sites 1098 and 1099 and to provide a stratigraphic framework for future investigators of the Palmer Deep to build upon.

ACKNOWLEDGMENTS

We are grateful to the Leg 178 laboratory technicians, whose careful curation of cores and data, core photography, and assistance with collection of many of the data sets made this and subsequent studies on the Palmer Deep cores possible. The manuscript benefited from the many useful suggestions that were provided by Tony Ramsay, John Farrell, and an anonymous reviewer. This project was funded by the United States Science Support Program of the Joint Oceanographic Institutions (JOI/USSSP grant F001154 at Texas A&M University) and by a National Science Foundation grant from the Office of Polar Programs (grant OPP-9615053 to Hamilton College). Data were provided courtesy of the Ocean Drilling Program.

REFERENCES

Alexandrovich, J.M., and Hays, J.D., 1989. High-resolution stratigraphic correlation of ODP Leg 111 Holes 677A and 677B and DSDP Leg 69 Hole 504. *In* Becker, K., Sakai, H., et al., *Proc. ODP, Sci. Results,* 111: College Station, TX (Ocean Drilling Program), 263–276.

Barker, P.F., Camerlenghi, A., Acton, G.D., et al., 1999. *Proc. ODP, Init. Repts.,*178 [CD-ROM]. Available from: Ocean Drilling Program, Texas A&M University, College Station, TX 77845-9547, USA.

Brachfeld, S., Acton, G.D., Guyodo, Y., and Banerjee, S.K., 2000. High-resolution paleomagnetic records from Holocene sediments from the Palmer Deep, western Antarctic Peninsula. *Earth Planet. Sci. Lett.,* 181:421–441.

Curry, W.B., Shackleton, N.J., Richter, C., et al., 1995. *Proc. ODP, Init. Repts.,* 154: College Station, TX (Ocean Drilling Program).

deMenocal, P., Bloemendal, J., and King, J., 1991. A rock-magnetic record of monsoonal dust deposition to the Arabian Sea: evidence for a shift in the mode of deposition at 2.4 Ma. *In* Prell, W.L., Niitsuma, N., et al., *Proc. ODP, Sci. Results,* 117: College Station, TX (Ocean Drilling Program), 389–407.

Farrell, J.W., and Janecek, T.R., 1991. Late Neogene paleoceanography and paleoclimatology of the northeast Indian Ocean (Site 758). *In* Weissel, J., Peirce, J., Taylor, E., Alt, J., et al., *Proc. ODP, Sci. Results,* 121: College Station, TX (Ocean Drilling Program), 297–355.

Gersonde, R., Hodell, D.A., Blum, P., et al., 1999. *Proc. ODP, Init. Repts.,* 177 [CD-ROM]. Available from: Ocean Drilling Program, Texas A&M University, College Station TX 77845-9547, USA.

Hagelberg, T., Shackleton, N., Pisias, N., and Shipboard Scientific Party, 1992. Development of composite depth sections for Sites 844 through 854. *In* Mayer, L., Pisias, N., Janecek, T., et al., *Proc. ODP, Init. Repts.,* 138 (Pt. 1): College Station, TX (Ocean Drilling Program), 79–85.

Hagelberg, T.K., Pisias, N.G., Shackleton, N.J., Mix, A.C., and Harris, S., 1995. Refinement of a high-resolution, continuous sedimentary section for studying equatorial Pacific Ocean paleoceanography, Leg 138. *In* Pisias, N.G., Mayer, L.A., Janecek, T.R., Palmer-Julson, A., and van Andel, T.H. (Eds.), *Proc. ODP, Sci Results,* 138: College Station, TX (Ocean Drilling Program), 31–46.

Harris, S., Hagelberg, T., Mix, A., Pisias, N.G., and Shackleton, N.J., 1995. Sediment depths determined by comparisons of GRAPE and logging density data during Leg 138. *In* Pisias, N.G., Mayer, L.A., Janecek, T.R., Palmer-Julson, A., and van Andel, T.H. (Eds.), *Proc. ODP, Sci. Results,* 138: College Station, TX (Ocean Drilling Program), 47–57.

Hvorslev, M.J., 1949. Subsurface exploration and sampling of soil for civil engineering purposes: report on a research project of the Committee on Sampling and Testing Soil Mechanics and Foundations Division. *Am. Soc. Civ. Eng., Waterways Experiment Station.*

Jansen, E., Raymo, M.E., Blum, P., et al., 1996. *Proc. ODP, Init. Repts.,* 162: College Station, TX (Ocean Drilling Program).

Keigwin, L.D., Rio, D., Acton, G.D., et al., 1998. *Proc. ODP, Init. Repts.,* 172: College Station, TX (Ocean Drilling Program).

Lyle, M., Koizumi, I., Richter, C., et al., 1997. *Proc. ODP, Init. Repts.,* 167: College Station, TX (Ocean Drilling Program).

MacKillop, A.K., Moran, K., Jarrett, K., Farrell, J., and Murray, D., 1995. Consolidation properties of equatorial Pacific Ocean sediments and their relationship to stress history and offsets in the Leg 138 composite depth sections. *In* Pisias, N.G., Mayer, L.A., Janecek, T.R., Palmer-Julson, A., and van Andel, T.H. (Eds.), *Proc. ODP, Sci. Results,* 138: College Station, TX (Ocean Drilling Program), 357–369.

Martinson, D.G., Menke, W., and Stoffa, P.L., 1982. An inverse approach to signal correlation. *J. Geophys. Res.,* 87:4807–4818.

Moran, K., 1997. Elastic property corrections applied to Leg 154 sediment, Ceara Rise. *In* Shackleton, N.J., Curry, W.B., Richter, C., and Bralower, T.J. (Eds.), *Proc. ODP, Sci. Results,* 154: College Station, TX (Ocean Drilling Program), 151–155.

Murray, D.W., and Prell, W.L., 1991. Pliocene to Pleistocene variations in calcium carbonate, organic carbon, and opal on the Owen Ridge, northern Arabian Sea. *In* Prell, W.L., Niitsuma, N., et al., *Proc. ODP, Sci. Results,* 117: College Station, TX (Ocean Drilling Program), 343–363.

Paillard, D., Labeyrie, L., and. Yiou, P., 1996. Macintosh program performs time-series analysis. *Eos,* 77:379.

Prell, W.L., Gardner, J.V., et al., 1982. *Init. Repts. DSDP,* 68: Washington (U.S. Govt. Printing Office).

Robinson, S.G., 1990. Applications for whole-core magnetic susceptibility measurements of deep-sea sediments: Leg 115 results. *In* Duncan, R.A., Backman, J., Peterson, L.C., et al., *Proc. ODP, Sci. Results,* 115: College Station, TX (Ocean Drilling Program), 737–771.

Ruddiman, W., Sarnthein, M., Baldauf, J., et al., 1988. *Proc. ODP, Init. Repts.,* 108 (Sections 1 and 2): College Station, TX (Ocean Drilling Program).

Ruddiman, W.F., Cameron, D., and Clement, B.M., 1987. Sediment disturbance and correlation of offset holes drilled with the hydraulic piston corer: Leg 94. *In* Ruddiman, W.F., Kidd, R.B., Thomas, E., et al., *Init. Repts. DSDP,* 94 (Pt. 2): Washington (U.S. Govt. Printing Office), 615–634.

Ruddiman, W.F., Kidd, R.B., Thomas, E., et al., 1987. *Init. Repts. DSDP,* 94 (Pts. 1 and 2): Washington (U.S. Govt. Printing Office).

Shackleton, N.J., Backman, J., Zimmerman, H., Kent, D.V., Hall, M.A., Roberts, D.G., Schnitker, D., Baldauf, J.G., Desprairies, A., Homrighausen, R., Huddlestun, P., Keene, J.B., Kaltenback, A.J., Krumsiek, K.A.O., Morton, A.C., Murray, J.W., and Westberg-Smith, J., 1984. Oxygen isotope calibration of the onset of ice-rafting and history of glaciation in the North Atlantic region. *Nature,* 307:620–623.

Wefer, G., Berger, W.H., and Richter, C., et al., 1998. *Proc. ODP, Init. Repts.,* 175: College Station, TX (Ocean Drilling Program).

Figure F1. Bathymetric map of Palmer Deep showing Leg 178 drill sites (modified from Barker, Camerlenghi, Acton, et al., 1999).

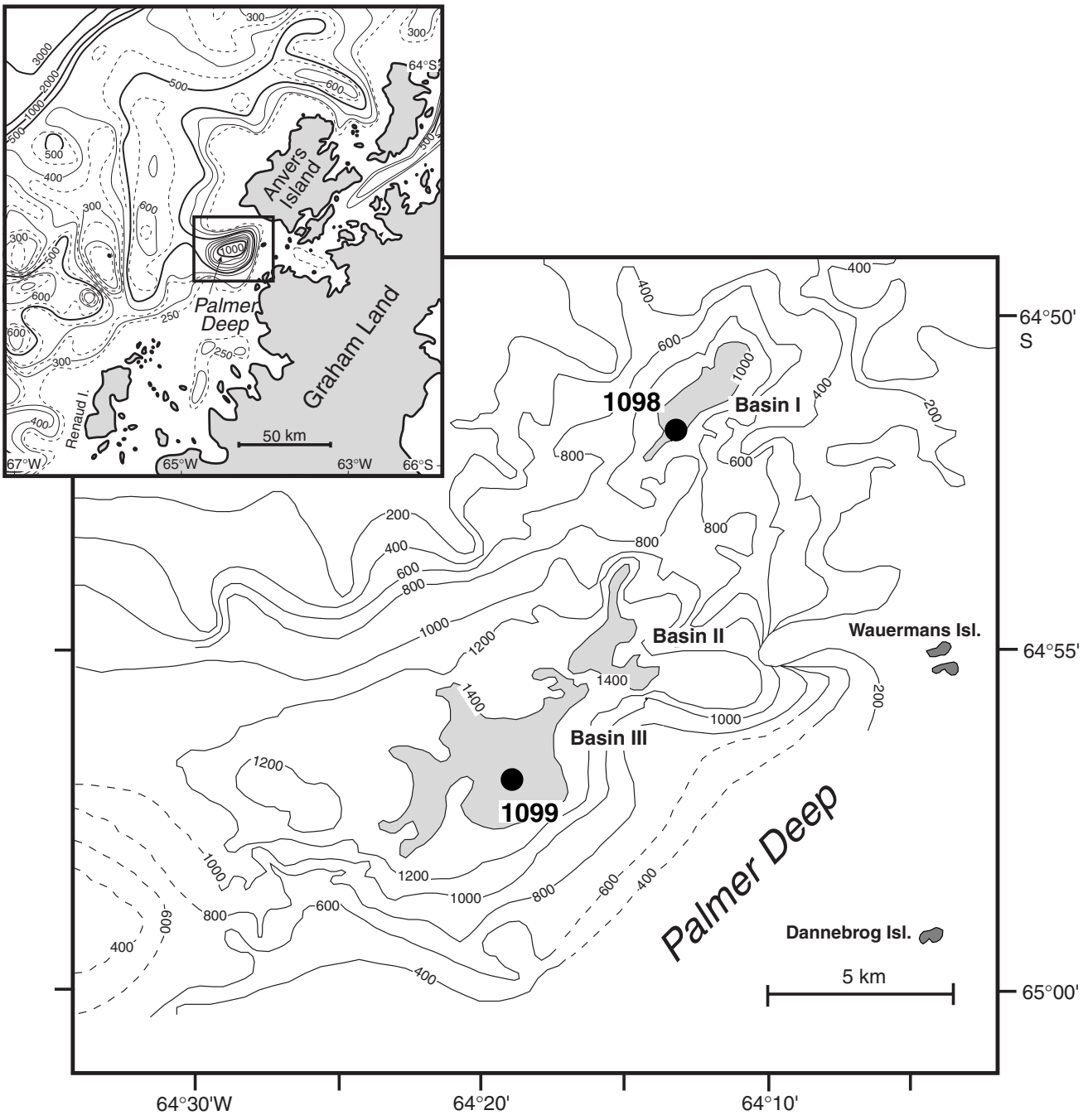

Figure F2. Susceptibility data on the mcd scale, Site 1098. All data were converted from raw meter units to volume SI units by multiplying by 0.7×10^{-5}. For viewing purposes, the Hole 1098B data were multiplied by 10, the Hole 1098C data by 100, and the spliced record by 10,000.

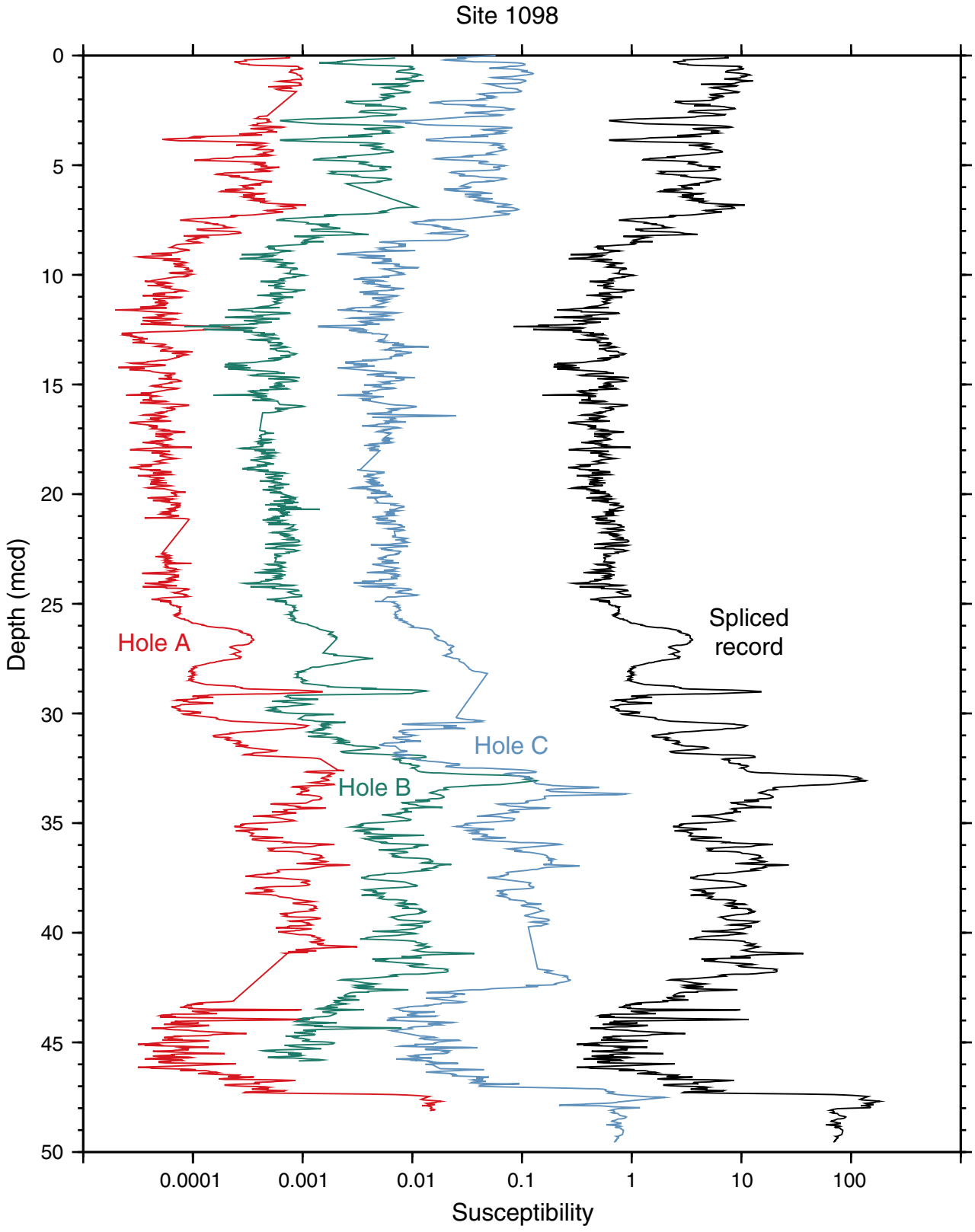

Figure F3. Susceptibility record on the mcd scale, 0–8 mcd, Site 1098. All data were converted from raw meter units to volume SI units by multiplying by 0.7×10^{-5}. For viewing purposes, the Hole 1098B data were multiplied by 10, the Hole 1098C data by 100, and the spliced record by 10,000.

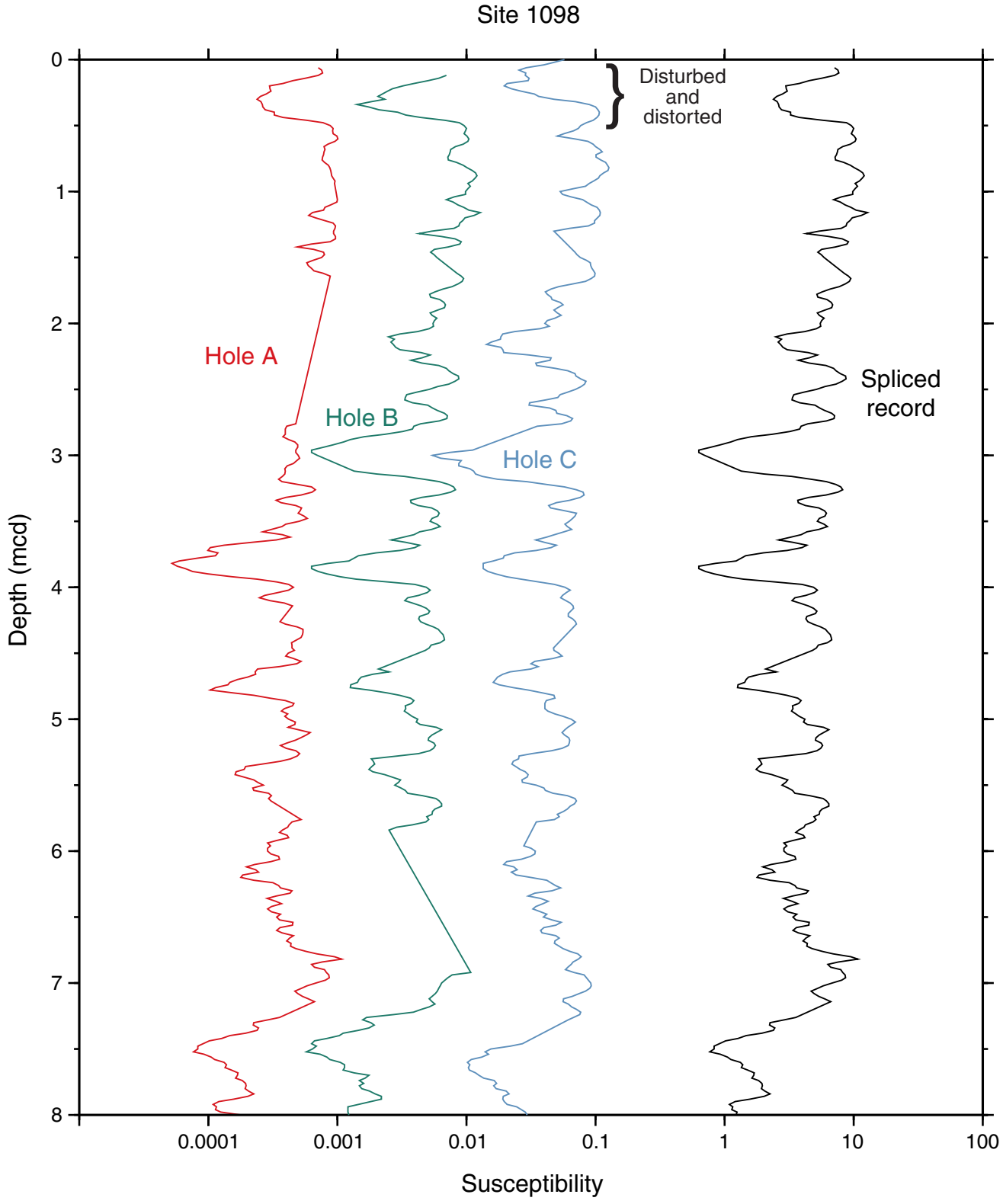

Figure F4. Susceptibility record on the mcd scale, 8–20 mcd, Site 1098. All data were converted from raw meter units to volume SI units by multiplying by 0.7×10^{-5}. For viewing purposes, the Hole 1098B data were multiplied by 10, the Hole 1098C data by 100, and the spliced record by 10,000.

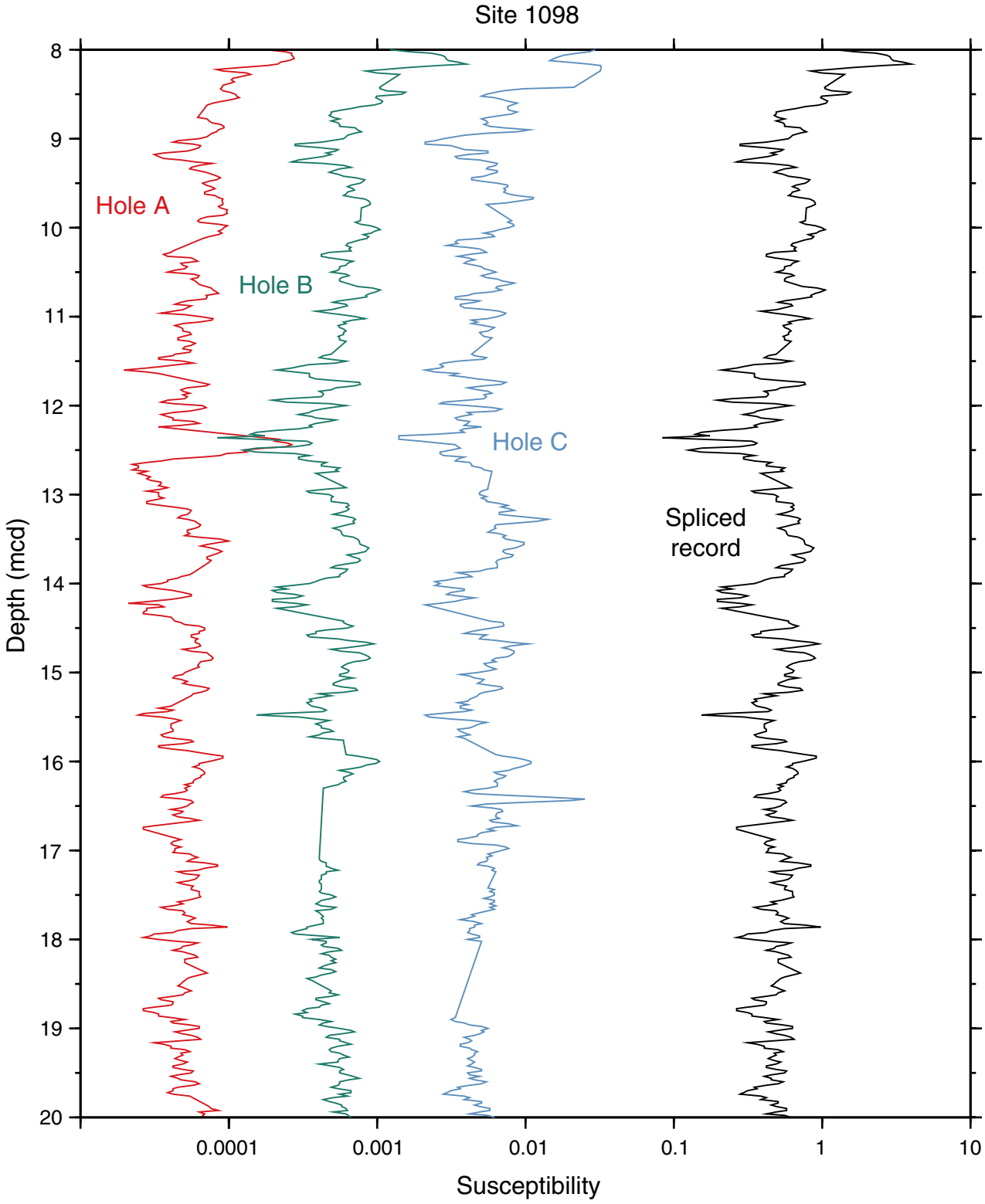

Figure F5. Susceptibility record on the mcd scale, 20–28 mcd, Site 1098. All data were converted from raw meter units to volume SI units by multiplying by 0.7×10^{-5}. For viewing purposes, the Hole 1098B data were multiplied by 10, the Hole 1098C data by 100, and the spliced record by 10,000.

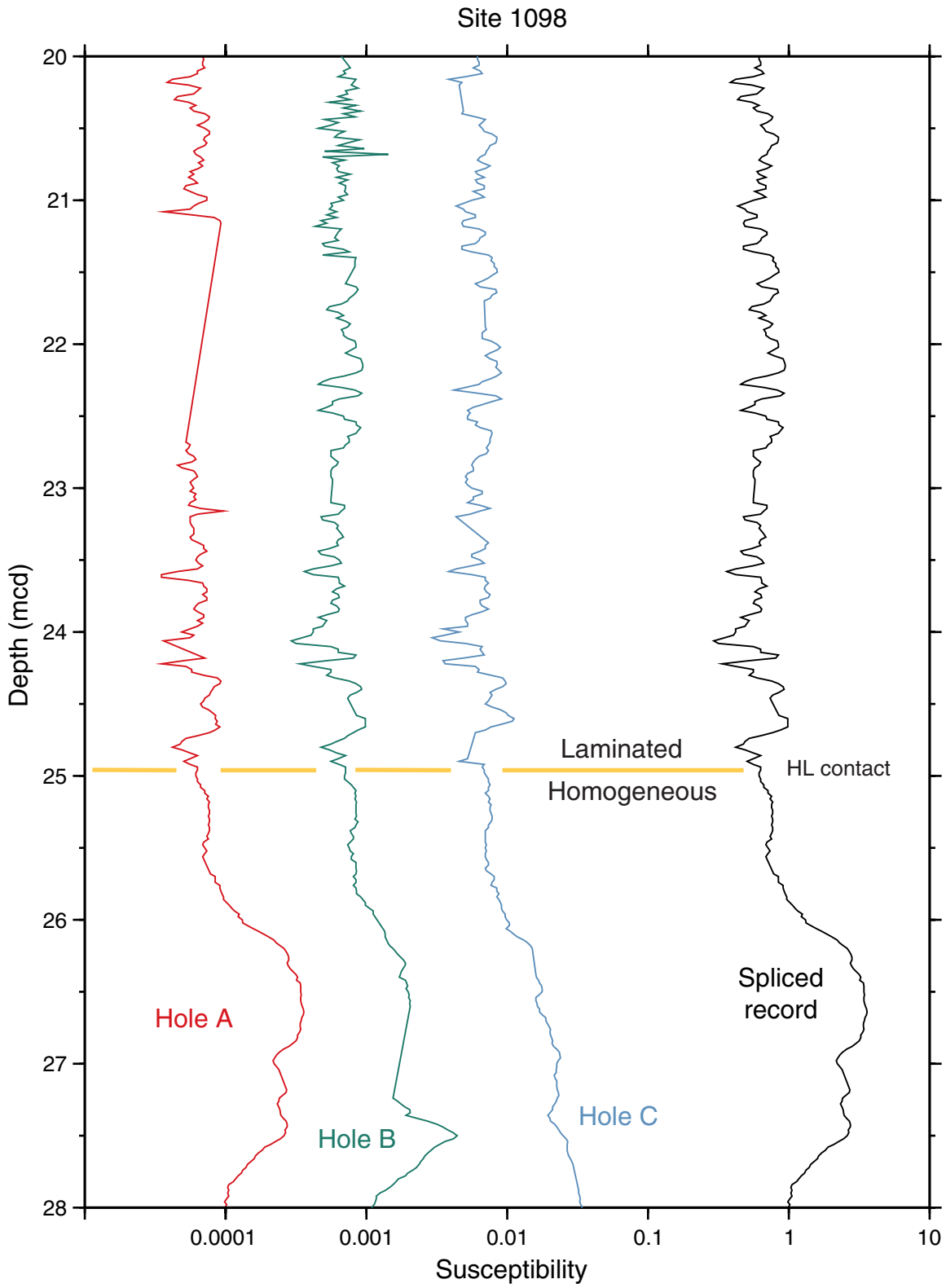

Figure F6. GRA density data on the mcd scale, Site 1098. For viewing purposes, 0.4 g/cm³ was added to the Hole 1098B data, 0.8 g/cm³ was added to the Hole 1098C data, and 1.6 g/cm³ was added to the spliced record.

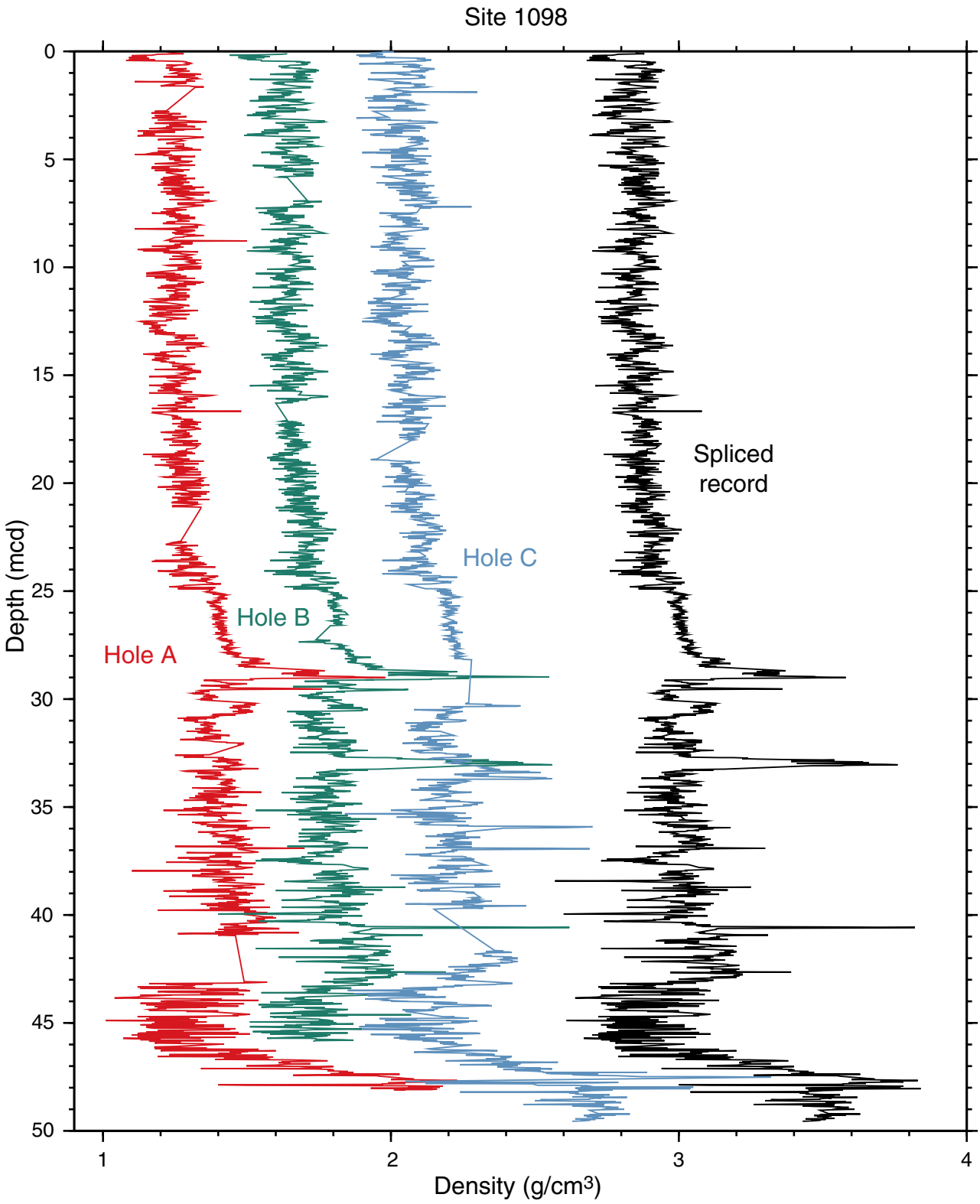

Figure F7. Density record on the mcd scale, 0–8 mcd, Site 1098. For viewing purposes, 0.4 g/cm³ was added to the Hole 1098B data, 0.8 g/cm³ was added to the Hole 1098C data, and 1.6 g/cm³ was added to the spliced record.

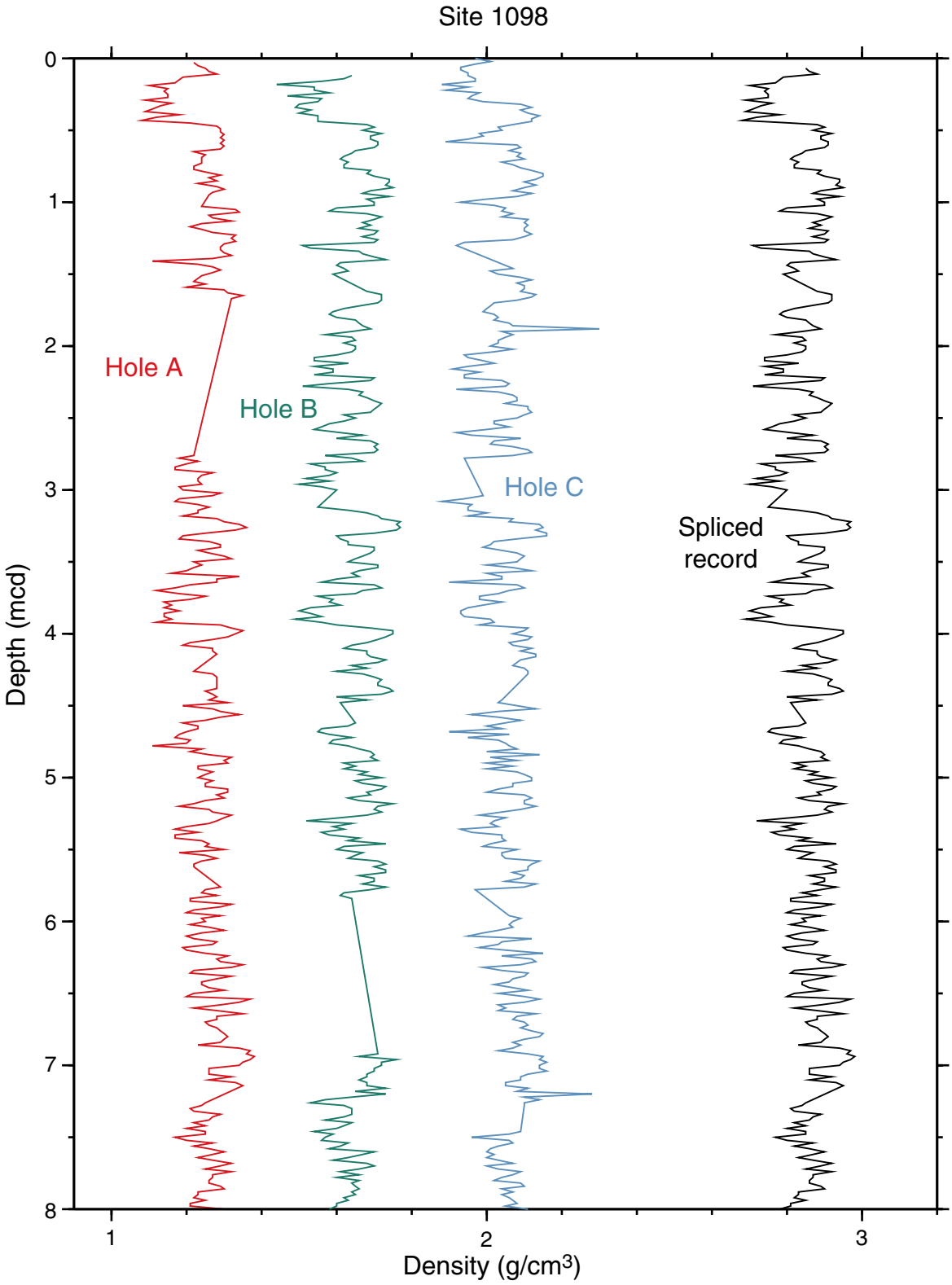

Figure F8. Density record on the mcd scale, 20–28 mcd, Site 1098. For viewing purposes, 0.4 g/cm³ was added to the Hole 1098B data, 0.8 g/cm³ was added to the Hole 1098C data, and 1.6 g/cm³ was added to the spliced record.

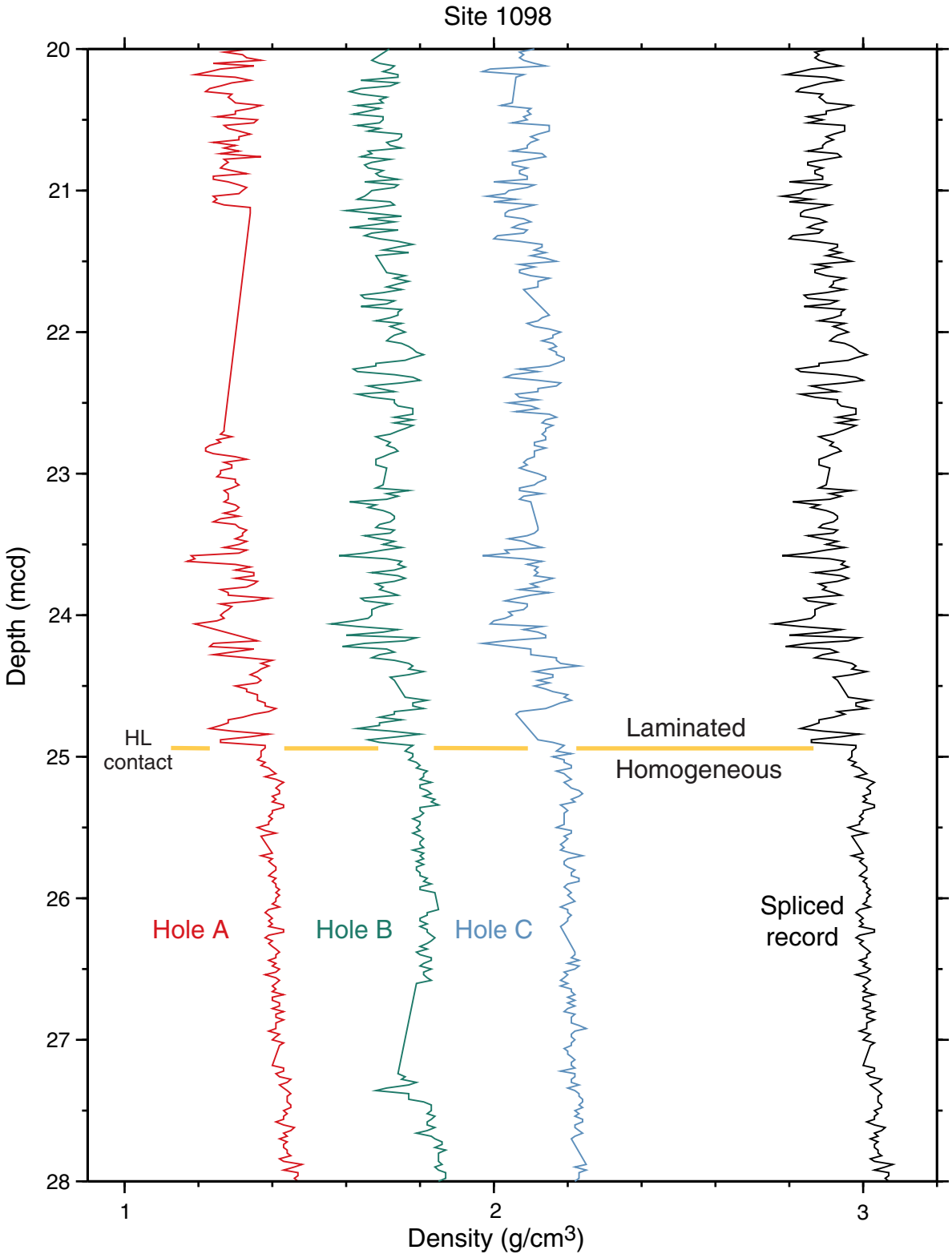

Figure F9. Density record on the mcd scale, 40–48 mcd, Site 1098. For viewing purposes, 0.4 g/cm³ was added to the Hole 1098B data, 0.8 g/cm³ was added to the Hole 1098C data, and 1.6 g/cm³ was added to the spliced record.

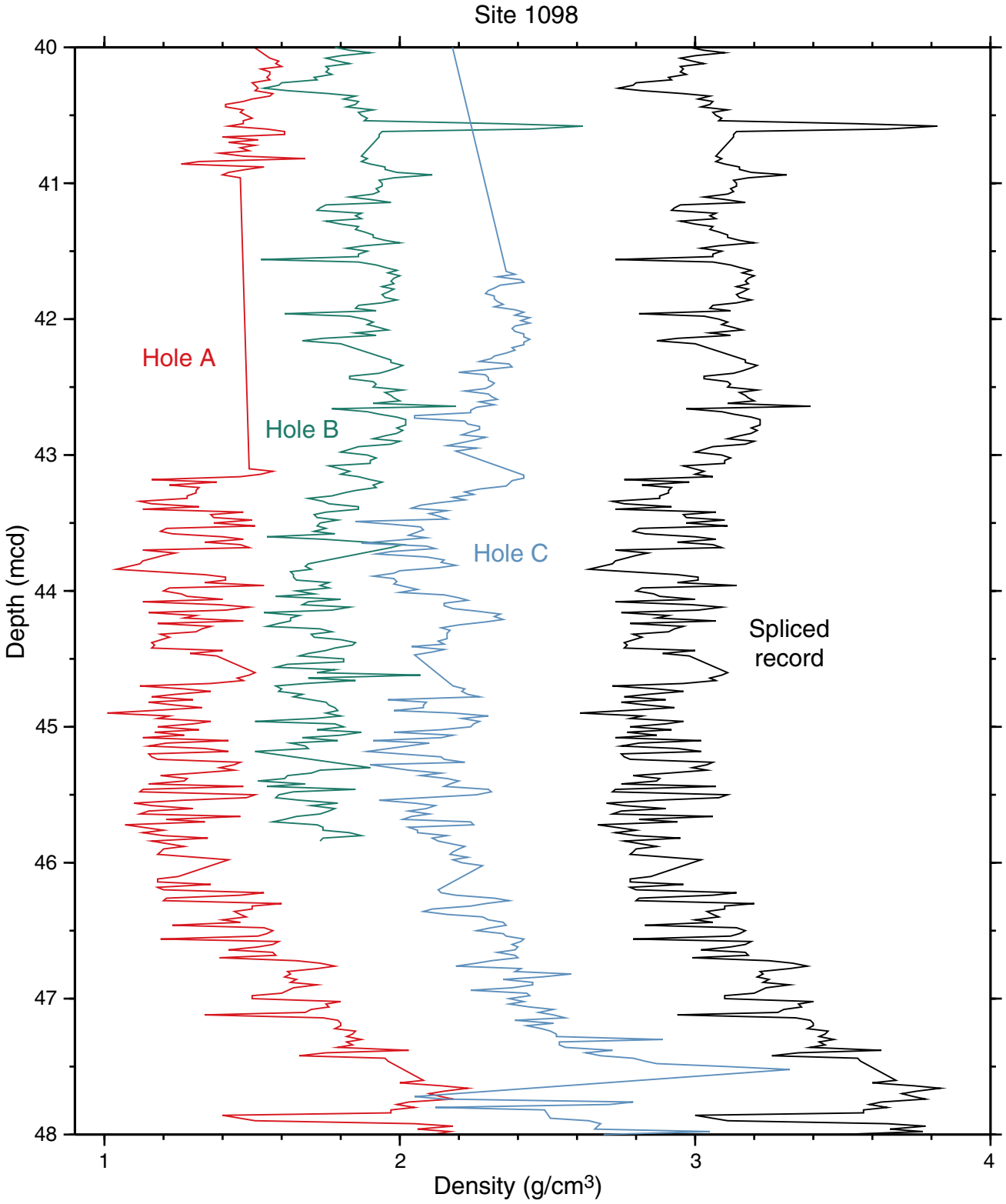

Figure F10. Magnetic intensity data, on the mcd scale, for Site 1098. For viewing purposes, the Hole 1098B data were multiplied by 10, the Hole 1098C data by 100, and the spliced record by 10,000.

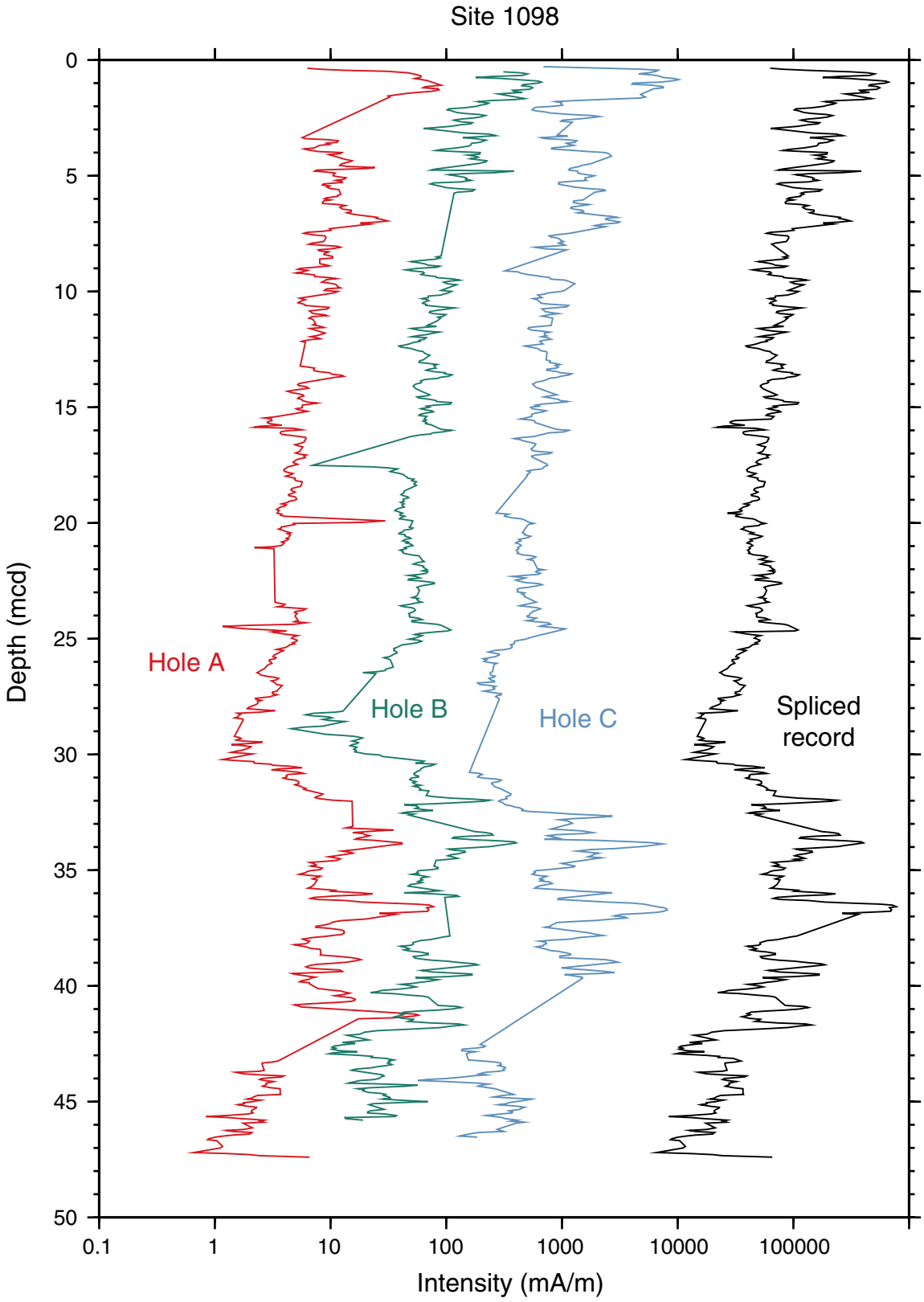

Figure F11. Magnetic intensity record on the mcd scale, 33–40 mcd, Site 1098. For viewing purposes, the Hole 1098B data were multiplied by 10, the Hole 1098C data by 100, and the spliced record by 10,000.

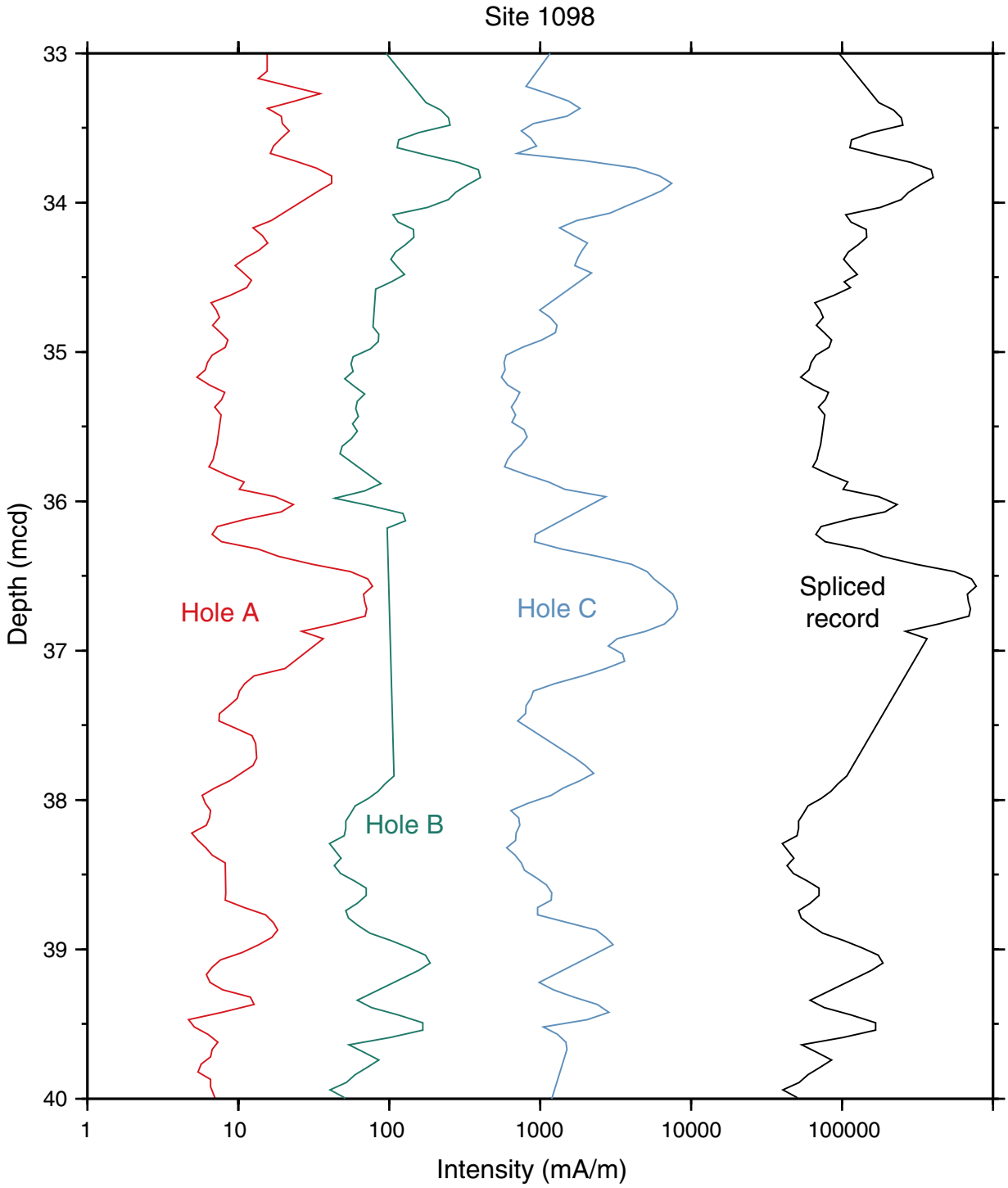

Figure F12. Color reflectance parameter a* data on the mcd scale for one of the better correlated intervals (20–28 mcd), Site 1098. For viewing purposes, 1.5 was added to the Hole 1098B data, 3.0 was added to the Hole 1098C data, and 5.5 was added to the spliced record.

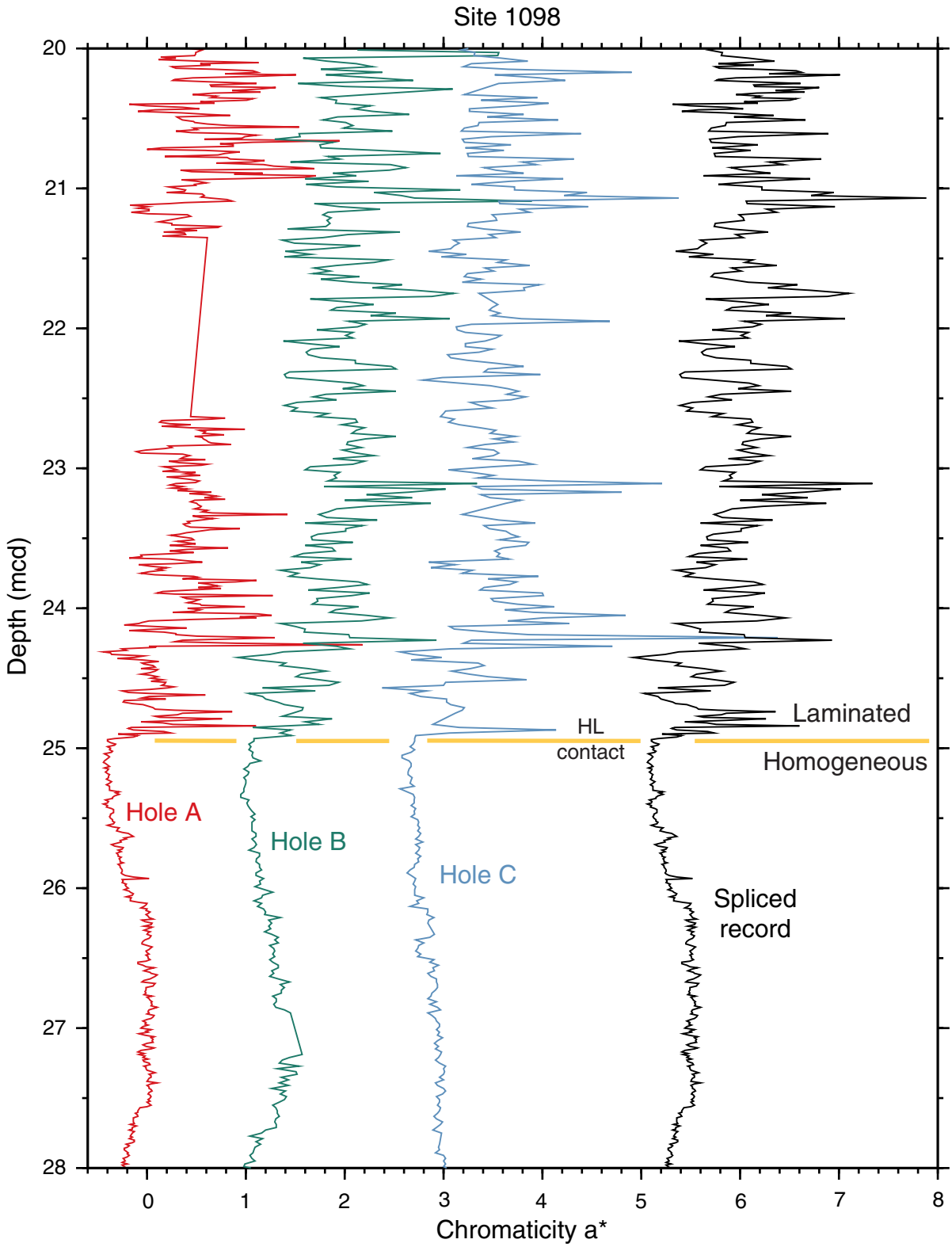

Figure F13. Illustration of the expansion of depth that occurs for the mcd scale relative to the mbsf scale, Site 1098.

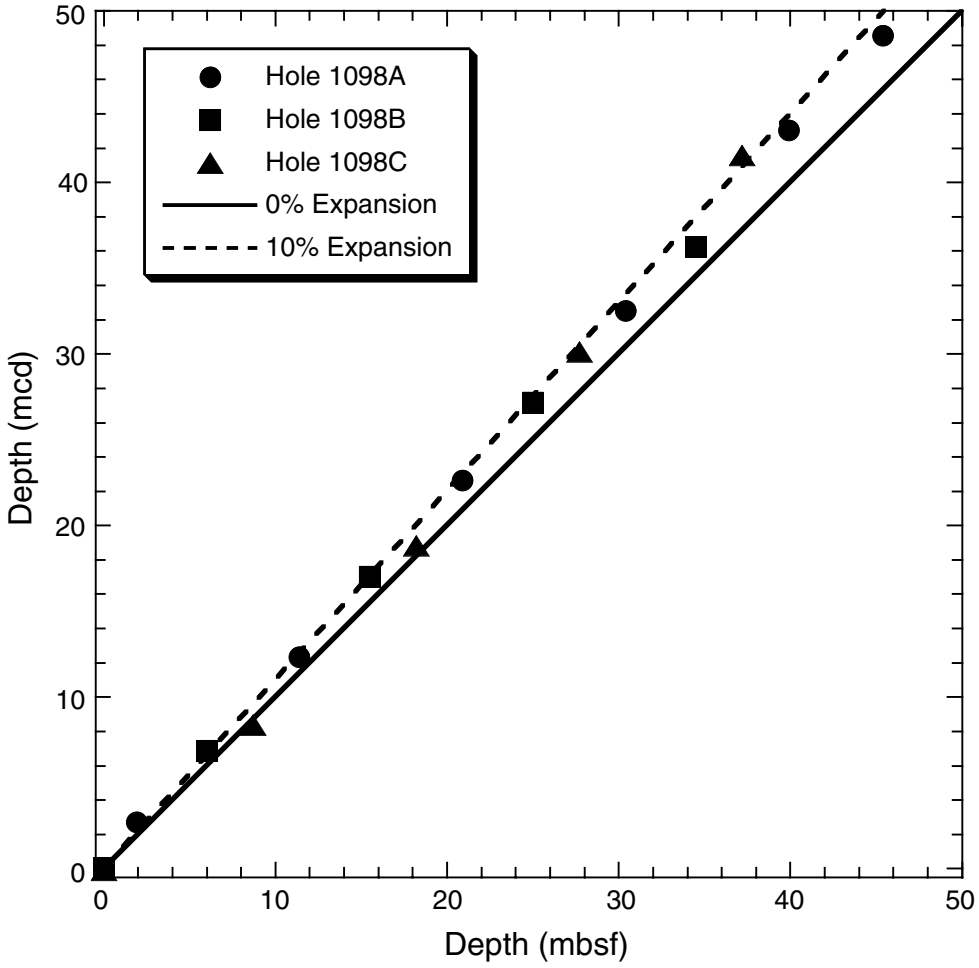

Table T1. Intervals disturbed or distorted by coring.

Section	Top of interval (cm)	Bottom of interval (cm)	Type of disturbance
178-1098A-			
2H-1	0	70	Top of core
3H-1	0	65	Top of core
4H-1	0	10	Top of core
5H-1	0	18	Top of core
178-1098B-			
3H-1	0	30	Top of core
4H-1	0	20	Top of core
5H-1	0	40	Top of core
178-1098C-			
1H-1	0	25	Top of core
2H-1	0	60	Top of core
3H-1	0	15	Top of core
4H-1	0	5	Top of core
5H-5	21	25	Void
178-1099A-			
2H-1	0	25	Top of core
4H-1	0	25	Top of core
6H-1	0	100	Top of core
7H-1	0	50	Top of core
7H-2	79	97	Void
7H-3	38	43	Void
7H-3	112	121	Void
7H-4	98	118	Void
178-1099B-			
1H-1	0	67	Top of core
1H-4	113	125	Void
1H-5	27	32	Void
2H-4	120	127	Void
2H-5	73	88	Void
3H-2	137	150	Void
3H-3	79	114	Void
3H-5	65	74	Void
3H-6	97	105	Void
4H-1	0	3	Top of core
4H-2	0	6	Void
4H-2	147	150	Void
4H-3	147	150	Void
4H-4	142	146	Void
5H-2	146	150	Void
5H-3	82	86	Void
5H-5	55	57	Void
5H-6	64	76	Void

Table T2. Composite depth scale, Site 1098.

Core	Depth (mbsf)	Depth (mcd)	Offset (mcd – mbsf)
178-1098A-			
1H	0.00	0.00	0.00
2H	1.90	2.70	0.80
3H	11.40	12.32	0.92
4H	20.90	22.62	1.72
5H	30.40	32.52	2.12
6H	39.90	43.04	3.14
7H	45.40	48.54	3.14
178-1098B-			
1H	0.00	0.06	0.06
2H	6.00	6.86	0.86
3H	15.50	17.02	1.52
4H	25.00	27.18	2.18
5H	34.50	36.24	1.74
178-1098C-			
1H	0.00	–0.10	–0.10
2H	8.70	8.36	–0.34
3H	18.20	18.82	0.62
4H	27.70	30.12	2.42
5H	37.20	41.59	4.39

Notes: mbsf = meters below seafloor, mcd = meters composite depth. Offset = amount added to the mbsf scale to get the mcd scale.

Table T3. Splice tie points, Site 1098.

Core, section, interval (cm)	Depth (mbsf)	Depth (mcd)	Type	Core, section, interval (cm)	Depth (mbsf)	Depth (mcd)
178-				178-		
1098A-1H-1, 46	0.46	0.46	Tie	1098B-1H-1, 40	0.40	0.46
1098B-1H-4, 122	5.72	5.78	Tie	1098A-2H-3, 8	4.98	5.78
1098A-2H-4, 78	7.18	7.98	Tie	1098B-2H-1, 112	7.12	7.98
1098B-2H-6, 118	14.68	15.54	Tie	1098A-3H-3, 22	14.62	15.54
1098A-3H-5, 124	18.64	19.56	Tie	1098C-3H-1, 74	18.94	19.56
1098C-3H-1, 130	19.50	20.12	Tie	1098A-3H-6, 30	19.20	20.12
1098A-3H-6, 66	19.56	20.48	Tie	1098C-3H-2, 16	19.86	20.48
1098C-3H-2, 134	21.04	21.66	Tie	1098B-3H-4, 14	20.14	21.66
1098B-3H-6, 16	23.16	24.68	Tie	1098A-4H-2, 56	22.96	24.68
1098A-4H-6, 130	29.70	31.42	Tie	1098B-4H-3, 124	29.24	31.42
1098B-4H-5, 138	32.38	34.56	Tie	1098A-5H-2, 54	32.44	34.56
1098A-5H-3, 144	34.84	36.96	Tie	1098B-5H-1, 72	35.22	36.96
1098B-5H-5, 90	41.40	43.14	Tie	1098A-6H-1, 10	40.00	43.14
1098A-6H-4, 44	44.84	47.98	Tie	1098C-5H-5, 34	43.59	47.98
1098C-5H-6, 42	45.17	49.56				

Table T4. Lithologic features used for correlating holes.

Lithologic feature description	Hole 1098A	Hole 1098B	Hole 1098C
HL contact	4H-2, 80 cm (23.20 mbsf; 24.92 mcd)	3H-6, 40 cm (23.40 mbsf; 24.92 mcd)	3H-5, 8 cm (24.28 mbsf; 24.90 mcd)
Upper LL diatomaceous mud contact	6H-1, 15 cm (40.05 mbsf; 43.19 mcd)	5H-5, 102 cm (41.52 mbsf; 43.26 mcd)	5H-2, 25 cm (38.95 mbsf; 43.34 mcd)
Subunit IA/IB contact	6H-3, 60 cm (43.50 mbsf; 46.64 mcd)	Not recovered	5H-4, 50 cm (42.25 mbsf; 46.64 mcd)

Note: HL = contact between a laminated diatom ooze and underlying very homogeneous massive diatom ooze, LL = lower laminated interval.

Table T5. Spliced magnetic susceptibility data.

Core, section, interval (cm)	Depth (mbsf)	Raw Susceptibility	Offset (m)	Depth (mcd)
178-1098A-1H-1				
6	0.06	101.20	0.00	0.06
8	0.08	108.20	0.00	0.08
10	0.10	109.50	0.00	0.10
12	0.12	101.50	0.00	0.12
14	0.14	81.00	0.00	0.14
16	0.16	64.80	0.00	0.16
18	0.18	54.20	0.00	0.18
20	0.20	42.50	0.00	0.20
22	0.22	43.00	0.00	0.22
24	0.24	43.50	0.00	0.24
26	0.26	40.00	0.00	0.26
28	0.28	36.20	0.00	0.28
30	0.30	34.00	0.00	0.30
32	0.32	36.50	0.00	0.32
34	0.34	37.50	0.00	0.34
36	0.36	37.80	0.00	0.36
38	0.38	39.50	0.00	0.38
40	0.40	46.50	0.00	0.40
42	0.42	46.20	0.00	0.42
44	0.44	54.20	0.00	0.44
46	0.46	83.00	0.00	0.46
178-1098B-1H-1				
42	0.42	125.20	0.06	0.48
44	0.44	136.80	0.06	0.50
46	0.46	143.20	0.06	0.52
48	0.48	141.00	0.06	0.54
50	0.50	137.20	0.06	0.56
52	0.52	144.20	0.06	0.58
54	0.54	149.00	0.06	0.60
56	0.56	147.00	0.06	0.62
58	0.58	134.20	0.06	0.64
60	0.60	117.00	0.06	0.66
62	0.62	107.50	0.06	0.68
64	0.64	107.00	0.06	0.70
66	0.66	104.80	0.06	0.72
68	0.68	102.50	0.06	0.74
70	0.70	103.20	0.06	0.76
72	0.72	119.20	0.06	0.78
74	0.74	134.80	0.06	0.80
76	0.76	144.50	0.06	0.82
78	0.78	157.80	0.06	0.84
80	0.80	168.50	0.06	0.86
82	0.82	172.00	0.06	0.88
84	0.84	166.80	0.06	0.90
86	0.86	158.20	0.06	0.92
88	0.88	146.80	0.06	0.94
90	0.90	152.80	0.06	0.96
92	0.92	146.20	0.06	0.98
94	0.94	140.00	0.06	1.00
96	0.96	140.20	0.06	1.02
98	0.98	115.00	0.06	1.04
100	1.00	100.00	0.06	1.06
102	1.02	112.20	0.06	1.08
104	1.04	122.50	0.06	1.10
106	1.06	135.20	0.06	1.12
108	1.08	149.20	0.06	1.14
110	1.10	183.00	0.06	1.16
112	1.12	163.20	0.06	1.18
114	1.14	139.20	0.06	1.20
116	1.16	133.80	0.06	1.22
118	1.18	127.20	0.06	1.24
120	1.20	124.80	0.06	1.26
122	1.22	114.00	0.06	1.28
124	1.24	76.50	0.06	1.30
126	1.26	61.20	0.06	1.32
128	1.28	90.80	0.06	1.34
130	1.30	116.80	0.06	1.36
132	1.32	130.20	0.06	1.38
134	1.34	127.20	0.06	1.40
136	1.36	103.00	0.06	1.42
138	1.38	80.80	0.06	1.44
140	1.40	75.50	0.06	1.46
142	1.42	80.00	0.06	1.48
144	1.44	84.50	0.06	1.50
178-1098B-1H-2				
6	1.56	120.20	0.06	1.62
8	1.58	130.20	0.06	1.64
10	1.60	136.00	0.06	1.66
12	1.62	132.80	0.06	1.68
14	1.64	124.00	0.06	1.70
16	1.66	111.00	0.06	1.72
18	1.68	94.00	0.06	1.74
20	1.70	81.50	0.06	1.76
22	1.72	74.00	0.06	1.78
24	1.74	75.20	0.06	1.80
26	1.76	88.80	0.06	1.82
28	1.78	95.50	0.06	1.84
30	1.80	98.00	0.06	1.86
32	1.82	96.20	0.06	1.88
34	1.84	85.50	0.06	1.90
36	1.86	75.00	0.06	1.92
38	1.88	77.50	0.06	1.94
40	1.90	84.50	0.06	1.96
42	1.92	81.00	0.06	1.98
44	1.94	78.50	0.06	2.00
46	1.96	79.00	0.06	2.02
48	1.98	73.20	0.06	2.04
50	2.00	59.80	0.06	2.06
52	2.02	43.80	0.06	2.08
54	2.04	35.50	0.06	2.10
56	2.06	39.50	0.06	2.12
58	2.08	37.00	0.06	2.14
60	2.10	38.80	0.06	2.16
62	2.12	40.50	0.06	2.18
64	2.14	43.80	0.06	2.20
66	2.16	63.50	0.06	2.22
68	2.18	74.80	0.06	2.24
70	2.20	64.80	0.06	2.26
72	2.22	53.00	0.06	2.28
74	2.24	64.80	0.06	2.30
76	2.26	86.80	0.06	2.32
78	2.28	100.20	0.06	2.34
80	2.30	104.50	0.06	2.36
82	2.32	112.20	0.06	2.38
84	2.34	123.80	0.06	2.40
86	2.36	125.00	0.06	2.42
88	2.38	116.80	0.06	2.44
90	2.40	104.20	0.06	2.46
92	2.42	86.00	0.06	2.48
94	2.44	73.20	0.06	2.50
96	2.46	58.50	0.06	2.52
98	2.48	49.00	0.06	2.54
100	2.50	48.00	0.06	2.56
102	2.52	47.50	0.06	2.58
104	2.54	54.50	0.06	2.60
106	2.56	71.50	0.06	2.62
108	2.58	77.80	0.06	2.64
110	2.60	85.00	0.06	2.66
112	2.62	96.80	0.06	2.68
114	2.64	101.80	0.06	2.70
116	2.66	100.80	0.06	2.72
118	2.68	87.80	0.06	2.74
120	2.70	63.00	0.06	2.76
122	2.72	55.80	0.06	2.78
124	2.74	54.50	0.06	2.80

Note: Only a portion of this table appears here. The complete table is available in **ASCII format.**

Table T6. Spliced GRA density data.

Core, section, interval (cm)	Depth (mbsf)	Density (g/cm^3)	Offset (m)	Depth (mcd)
178-1098A-1H-1				
7	0.07	1.25	0.00	0.07
9	0.09	1.26	0.00	0.09
11	0.11	1.28	0.00	0.11
13	0.13	1.19	0.00	0.13
15	0.15	1.18	0.00	0.15
17	0.17	1.17	0.00	0.17
19	0.19	1.10	0.00	0.19
21	0.21	1.15	0.00	0.21
23	0.23	1.14	0.00	0.23
25	0.25	1.15	0.00	0.25
27	0.27	1.15	0.00	0.27
29	0.29	1.09	0.00	0.29
31	0.31	1.16	0.00	0.31
33	0.33	1.13	0.00	0.33
35	0.35	1.11	0.00	0.35
37	0.37	1.09	0.00	0.37
39	0.39	1.18	0.00	0.39
41	0.41	1.12	0.00	0.41
43	0.43	1.08	0.00	0.43
45	0.45	1.21	0.00	0.45
40	0.40	1.28	0.06	0.46
42	0.42	1.30	0.06	0.48
44	0.44	1.27	0.06	0.50
46	0.46	1.32	0.06	0.52
48	0.48	1.29	0.06	0.54
50	0.50	1.29	0.06	0.56
52	0.52	1.31	0.06	0.58
54	0.54	1.31	0.06	0.60
56	0.56	1.30	0.06	0.62
58	0.58	1.25	0.06	0.64
60	0.60	1.24	0.06	0.66
62	0.62	1.22	0.06	0.68
64	0.64	1.21	0.06	0.70
66	0.66	1.23	0.06	0.72
68	0.68	1.22	0.06	0.74
70	0.70	1.22	0.06	0.76
72	0.72	1.29	0.06	0.78
74	0.74	1.28	0.06	0.80
76	0.76	1.30	0.06	0.82
78	0.78	1.34	0.06	0.84
80	0.80	1.34	0.06	0.86
82	0.82	1.33	0.06	0.88
84	0.84	1.35	0.06	0.90
86	0.86	1.29	0.06	0.92
88	0.88	1.27	0.06	0.94
90	0.90	1.34	0.06	0.96
92	0.92	1.28	0.06	0.98
94	0.94	1.30	0.06	1.00
96	0.96	1.30	0.06	1.02
98	0.98	1.20	0.06	1.04
100	1.00	1.18	0.06	1.06
102	1.02	1.28	0.06	1.08
104	1.04	1.32	0.06	1.10
106	1.06	1.30	0.06	1.12
108	1.08	1.27	0.06	1.14
110	1.10	1.29	0.06	1.16
112	1.12	1.26	0.06	1.18
114	1.14	1.31	0.06	1.20
116	1.16	1.30	0.06	1.22
118	1.18	1.27	0.06	1.24
120	1.20	1.31	0.06	1.26
122	1.22	1.30	0.06	1.28
124	1.24	1.11	0.06	1.30
126	1.26	1.13	0.06	1.32
128	1.28	1.26	0.06	1.34
130	1.30	1.27	0.06	1.36
132	1.32	1.30	0.06	1.38
134	1.34	1.33	0.06	1.40
136	1.36	1.21	0.06	1.42
138	1.38	1.20	0.06	1.44
140	1.40	1.22	0.06	1.46
142	1.42	1.23	0.06	1.48
144	1.44	1.19	0.06	1.50
178-1098B-1H-2				
6	1.56	1.28	0.06	1.62
8	1.58	1.32	0.06	1.64
10	1.60	1.32	0.06	1.66
12	1.62	1.32	0.06	1.68
14	1.64	1.31	0.06	1.70
16	1.66	1.26	0.06	1.72
18	1.68	1.22	0.06	1.74
20	1.70	1.19	0.06	1.76
22	1.72	1.18	0.06	1.78
24	1.74	1.20	0.06	1.80
26	1.76	1.25	0.06	1.82
28	1.78	1.26	0.06	1.84
30	1.80	1.27	0.06	1.86
32	1.82	1.29	0.06	1.88
34	1.84	1.24	0.06	1.90
36	1.86	1.17	0.06	1.92
38	1.88	1.24	0.06	1.94
40	1.90	1.25	0.06	1.96
42	1.92	1.22	0.06	1.98
44	1.94	1.25	0.06	2.00
46	1.96	1.25	0.06	2.02
48	1.98	1.24	0.06	2.04
50	2.00	1.20	0.06	2.06
52	2.02	1.14	0.06	2.08
54	2.04	1.14	0.06	2.10
56	2.06	1.23	0.06	2.12
58	2.08	1.14	0.06	2.14
60	2.10	1.19	0.06	2.16
62	2.12	1.19	0.06	2.18
64	2.14	1.14	0.06	2.20
66	2.16	1.30	0.06	2.22
68	2.18	1.29	0.06	2.24
70	2.20	1.18	0.06	2.26
72	2.22	1.11	0.06	2.28
74	2.24	1.23	0.06	2.30
76	2.26	1.27	0.06	2.32
78	2.28	1.26	0.06	2.34
80	2.30	1.28	0.06	2.36
82	2.32	1.30	0.06	2.38
84	2.34	1.32	0.06	2.40
86	2.36	1.31	0.06	2.42
88	2.38	1.30	0.06	2.44
90	2.40	1.29	0.06	2.46
92	2.42	1.22	0.06	2.48
94	2.44	1.25	0.06	2.50
96	2.46	1.22	0.06	2.52
98	2.48	1.18	0.06	2.54
100	2.50	1.16	0.06	2.56
102	2.52	1.14	0.06	2.58
104	2.54	1.21	0.06	2.60
106	2.56	1.27	0.06	2.62
108	2.58	1.20	0.06	2.64
110	2.60	1.29	0.06	2.66
112	2.62	1.31	0.06	2.68
114	2.64	1.30	0.06	2.70
116	2.66	1.31	0.06	2.72
118	2.68	1.30	0.06	2.74
120	2.70	1.17	0.06	2.76
122	2.72	1.24	0.06	2.78

Note: Only a portion of this table appears here. The complete table is available in **ASCII format.**

Table T7. Spliced magnetic intensity data.

Core, section, interval (cm)	Depth (mbsf)	Intensity (mA/m)	Offset (m)	Depth (mcd)
178-1098A-1H-1				
35	0.35	6.28	0.00	0.35
40	0.40	8.15	0.00	0.40
45	0.45	12.80	0.00	0.45
178-1098B-1H-1				
45	0.45	31.23	0.06	0.51
50	0.50	44.27	0.06	0.56
55	0.55	50.60	0.06	0.61
60	0.60	45.38	0.06	0.66
65	0.65	25.01	0.06	0.71
70	0.70	17.96	0.06	0.76
75	0.75	30.74	0.06	0.81
80	0.80	46.34	0.06	0.86
85	0.85	62.14	0.06	0.91
90	0.90	66.18	0.06	0.96
95	0.95	62.04	0.06	1.01
100	1.00	45.79	0.06	1.06
105	1.05	44.84	0.06	1.11
110	1.10	53.61	0.06	1.16
115	1.15	55.74	0.06	1.21
120	1.20	52.62	0.06	1.26
125	1.25	37.41	0.06	1.31
130	1.30	38.55	0.06	1.36
135	1.35	45.26	0.06	1.41
140	1.40	28.11	0.06	1.46
178-1098B-1H-2				
10	1.60	47.54	0.06	1.66
15	1.65	39.53	0.06	1.71
20	1.70	23.74	0.06	1.76
25	1.75	18.84	0.06	1.81
30	1.80	23.10	0.06	1.86
35	1.85	21.92	0.06	1.91
40	1.90	19.56	0.06	1.96
45	1.95	18.24	0.06	2.01
50	2.00	14.26	0.06	2.06
55	2.05	10.53	0.06	2.11
60	2.10	10.24	0.06	2.16
65	2.15	11.20	0.06	2.21
70	2.20	12.25	0.06	2.26
75	2.25	14.48	0.06	2.31
80	2.30	19.24	0.06	2.36
85	2.35	21.67	0.06	2.41
90	2.40	19.57	0.06	2.46
95	2.45	16.64	0.06	2.51
100	2.50	13.12	0.06	2.56
105	2.55	11.67	0.06	2.61
110	2.60	13.28	0.06	2.66
115	2.65	16.82	0.06	2.71
120	2.70	16.37	0.06	2.76
125	2.75	13.38	0.06	2.81
130	2.80	10.82	0.06	2.86
135	2.85	8.52	0.06	2.91
140	2.90	6.35	0.06	2.96
178-1098B-1H-3				
10	3.10	14.66	0.06	3.16
15	3.15	23.36	0.06	3.21
20	3.20	26.77	0.06	3.26
25	3.25	20.00	0.06	3.31
30	3.30	13.91	0.06	3.36
35	3.35	18.01	0.06	3.41
40	3.40	21.90	0.06	3.46
45	3.45	20.70	0.06	3.51
50	3.50	19.71	0.06	3.56
55	3.55	16.49	0.06	3.61
60	3.60	16.26	0.06	3.66
65	3.65	15.84	0.06	3.71
70	3.70	14.04	0.06	3.76
75	3.75	12.25	0.06	3.81
80	3.80	9.01	0.06	3.86
85	3.85	8.14	0.06	3.91
90	3.90	12.06	0.06	3.96
95	3.95	19.66	0.06	4.01
100	4.00	19.49	0.06	4.06
105	4.05	15.30	0.06	4.11
110	4.10	17.67	0.06	4.16
115	4.15	18.95	0.06	4.21
120	4.20	16.16	0.06	4.26
125	4.25	18.85	0.06	4.31
130	4.30	22.34	0.06	4.36
135	4.35	22.05	0.06	4.41
140	4.40	19.30	0.06	4.46
178-1098B-1H-4				
10	4.60	9.48	0.06	4.66
15	4.65	8.05	0.06	4.71
20	4.70	7.45	0.06	4.76
25	4.75	38.43	0.06	4.81
30	4.80	26.72	0.06	4.86
35	4.85	13.91	0.06	4.91
40	4.90	10.51	0.06	4.96
45	4.95	11.92	0.06	5.01
50	5.00	14.30	0.06	5.06
55	5.05	15.10	0.06	5.11
60	5.10	14.68	0.06	5.16
65	5.15	16.40	0.06	5.21
70	5.20	13.51	0.06	5.26
75	5.25	7.78	0.06	5.31
80	5.30	7.28	0.06	5.36
85	5.35	8.00	0.06	5.41
90	5.40	9.16	0.06	5.46
95	5.45	9.87	0.06	5.51
100	5.50	12.33	0.06	5.56
105	5.55	17.52	0.06	5.61
110	5.60	16.82	0.06	5.66
115	5.65	12.57	0.06	5.71
120	5.70	11.71	0.06	5.76
178-1098A-2H-3				
10	5.00	12.30	0.80	5.80
15	5.05	11.50	0.80	5.85
20	5.10	11.50	0.80	5.90
25	5.15	9.20	0.80	5.95
30	5.20	8.84	0.80	6.00
35	5.25	9.96	0.80	6.05
40	5.30	8.79	0.80	6.10
45	5.35	8.45	0.80	6.15
50	5.40	8.61	0.80	6.20
55	5.45	11.70	0.80	6.25
60	5.50	13.40	0.80	6.30
65	5.55	12.00	0.80	6.35
70	5.60	12.30	0.80	6.40
75	5.65	12.80	0.80	6.45
80	5.70	15.00	0.80	6.50
85	5.75	15.00	0.80	6.55
90	5.80	13.90	0.80	6.60
95	5.85	15.10	0.80	6.65
100	5.90	16.90	0.80	6.70
105	5.95	21.80	0.80	6.75
110	6.00	25.40	0.80	6.80
115	6.05	24.90	0.80	6.85
120	6.10	27.80	0.80	6.90
125	6.15	31.00	0.80	6.95
130	6.20	25.50	0.80	7.00
135	6.25	18.10	0.80	7.05
140	6.30	21.90	0.80	7.10

Note: Only a portion of this table appears here. The complete table is available in **ASCII format.**

Table T8. Spliced color reflectance parameter a* data.

Core, section, interval (cm)	Depth (mbsf)	a*	Offset (m)	Depth (mcd)
178-1098A-1H-1				
7	0.07	1.03	0.00	0.07
9	0.09	0.99	0.00	0.09
11	0.11	1.37	0.00	0.11
13	0.13	1.55	0.00	0.13
15	0.15	1.57	0.00	0.15
17	0.17	1.76	0.00	0.17
19	0.19	1.72	0.00	0.19
21	0.21	1.32	0.00	0.21
23	0.23	0.64	0.00	0.23
25	0.25	0.75	0.00	0.25
27	0.27	1.02	0.00	0.27
29	0.29	0.59	0.00	0.29
31	0.31	0.19	0.00	0.31
33	0.33	0.44	0.00	0.33
35	0.35	0.32	0.00	0.35
37	0.37	–0.13	0.00	0.37
39	0.39	–0.16	0.00	0.39
41	0.41	0.19	0.00	0.41
43	0.43	0.40	0.00	0.43
45	0.45	–0.26	0.00	0.45
178-1098B-1H-1				
40	0.40	0.16	0.06	0.46
41	0.41	0.75	0.06	0.47
42	0.42	1.09	0.06	0.48
43	0.43	0.49	0.06	0.49
44	0.44	0.26	0.06	0.50
45	0.45	0.44	0.06	0.51
46	0.46	0.62	0.06	0.52
47	0.47	0.69	0.06	0.53
48	0.48	0.74	0.06	0.54
49	0.49	0.80	0.06	0.55
50	0.50	0.97	0.06	0.56
51	0.51	1.07	0.06	0.57
52	0.52	1.10	0.06	0.58
53	0.53	1.04	0.06	0.59
54	0.54	1.08	0.06	0.60
55	0.55	1.11	0.06	0.61
56	0.56	1.11	0.06	0.62
57	0.57	1.19	0.06	0.63
58	0.58	1.10	0.06	0.64
59	0.59	0.99	0.06	0.65
60	0.60	1.31	0.06	0.66
61	0.61	1.30	0.06	0.67
62	0.62	1.12	0.06	0.68
63	0.63	0.82	0.06	0.69
64	0.64	0.91	0.06	0.70
65	0.65	0.99	0.06	0.71
66	0.66	0.69	0.06	0.72
67	0.67	0.76	0.06	0.73
68	0.68	0.83	0.06	0.74
69	0.69	0.68	0.06	0.75
70	0.70	–0.20	0.06	0.76
71	0.71	0.00	0.06	0.77
72	0.72	0.28	0.06	0.78
73	0.73	0.93	0.06	0.79
74	0.74	0.72	0.06	0.80
75	0.75	0.84	0.06	0.81
76	0.76	0.86	0.06	0.82
77	0.77	0.62	0.06	0.83
78	0.78	0.50	0.06	0.84
79	0.79	0.56	0.06	0.85
80	0.80	0.54	0.06	0.86
81	0.81	0.64	0.06	0.87
82	0.82	0.85	0.06	0.88
83	0.83	0.95	0.06	0.89
84	0.84	0.98	0.06	0.90
85	0.85	0.83	0.06	0.91
86	0.86	0.90	0.06	0.92
87	0.87	0.93	0.06	0.93
88	0.88	1.23	0.06	0.94
89	0.89	0.58	0.06	0.95
90	0.90	0.64	0.06	0.96
91	0.91	0.76	0.06	0.97
92	0.92	0.92	0.06	0.98
93	0.93	0.99	0.06	0.99
94	0.94	1.23	0.06	1.00
95	0.95	0.59	0.06	1.01
96	0.96	0.51	0.06	1.02
97	0.97	1.09	0.06	1.03
98	0.98	1.17	0.06	1.04
99	0.99	1.33	0.06	1.05
100	1.00	0.93	0.06	1.06
101	1.01	0.66	0.06	1.07
102	1.02	0.52	0.06	1.08
103	1.03	0.69	0.06	1.09
104	1.04	0.86	0.06	1.10
105	1.05	0.52	0.06	1.11
106	1.06	0.73	0.06	1.12
107	1.07	0.70	0.06	1.13
108	1.08	1.08	0.06	1.14
109	1.09	0.89	0.06	1.15
110	1.10	1.07	0.06	1.16
111	1.11	1.08	0.06	1.17
112	1.12	1.25	0.06	1.18
113	1.13	0.99	0.06	1.19
114	1.14	1.01	0.06	1.20
115	1.15	1.11	0.06	1.21
116	1.16	1.10	0.06	1.22
117	1.17	1.10	0.06	1.23
118	1.18	1.04	0.06	1.24
119	1.19	0.80	0.06	1.25
120	1.20	0.80	0.06	1.26
121	1.21	1.00	0.06	1.27
122	1.22	0.99	0.06	1.28
123	1.23	1.15	0.06	1.29
124	1.24	1.33	0.06	1.30
125	1.25	1.39	0.06	1.31
126	1.26	2.97	0.06	1.32
127	1.27	1.85	0.06	1.33
128	1.28	0.57	0.06	1.34
129	1.29	0.00	0.06	1.35
130	1.30	0.10	0.06	1.36
131	1.31	0.13	0.06	1.37
132	1.32	0.38	0.06	1.38
133	1.33	0.54	0.06	1.39
134	1.34	1.04	0.06	1.40
135	1.35	1.12	0.06	1.41
136	1.36	1.14	0.06	1.42
137	1.37	0.98	0.06	1.43
138	1.38	0.82	0.06	1.44
139	1.39	0.72	0.06	1.45
140	1.40	0.83	0.06	1.46
141	1.41	0.70	0.06	1.47
142	1.42	1.26	0.06	1.48
143	1.43	0.65	0.06	1.49
144	1.44	0.92	0.06	1.50
145	1.45	1.16	0.06	1.51
146	1.46	0.95	0.06	1.52
147	1.47	0.84	0.06	1.53
148	1.48	0.76	0.06	1.54

Note: Only a portion of this table appears here. The complete table is available in **ASCII format.**